2009

BIOACTIVE SCAFFOLDS FOR TISSUE ENGINEERING

Jason P. Haley

BIOACTIVE SCAFFOLDS FOR TISSUE ENGINEERING

(Thesis format: Monograph)

by

Jason P. Haley

Graduate Program in Biomedical Engineering

A thesis submitted in partial fulfillment
of the requirements for the degree of
Master of Engineering Science

The School of Graduate and Postdoctoral Studies
The University of Western Ontario
London, Ontario, Canada

ABSTRACT

Tissue engineering is recognized as a promising alternative to conventional reconstructive materials and donor tissues, which are in short supply. The effective use of nanofibers as tissue scaffolds relies on the localized delivery of signaling proteins, providing biochemical cues for tissue regeneration. This study aimed to fabricate bioactive scaffolds by incorporating proteins for controlled release through a coaxial electrospinning process. It was used to fabricate Poly (ε-Caprolactone) fibers within which bioactive proteins were encapsulated. Scaffolds were characterized using SEM and confocal microscopy to verify uniformity and continuity of protein encapsulation. Protein release kinetics were evaluated using fluorescence spectroscopy and a Bradford protein assay. Cell culture studies using radial arterial cells were performed on scaffolds containing either TGF-β1 or PDGF-BB. The protein release study suggested diffusive transport was sustained over a 72-hour period and significantly improved cell proliferation. The present results provide a basis for further optimization of scaffold processing parameters.

Keywords: *tissue engineering, coaxial electrospinning, poly (ε-caprolactone), transforming growth factor, platelet derived growth factor, radial arterial cells.*

ACKNOWLEDGMENTS

I would like to express my sincere thanks and gratitude to all of those who helped make this thesis possible. I am particularly grateful for the guidance and encouragement of my supervisors, Dr. Wankei Wan and Dr. Derek Boughner. I am wholeheartedly appreciative of their ongoing support and insightful discussions enabling me to carry out this research.

The support from my colleagues has been instrumental in facilitating various portions of the work carried out throughout this thesis. I would like to thank Mina Mekhail for introducing me to electrospinning; Zachary Armstrong for teaching me cell seeding and staining techniques; Kenneth Wong for acquiring scanning electron microscopy images; Christine Oates for technical support with the fluorescence reader; Karen Kennedy for assistance with the ELISA and everyone else in Dr. Wan's lab for their technical advice and valuable friendship.

I would like to thank the Heart and Stroke Foundation of Ontario (HSFO) and the Canadian Institutes of Health Research (CIHR) for their financial support.

I am sincerely grateful for the love and support of my family. They have provided me with the encouragement and perseverance to accomplish this thesis. Finally, I would like to give a special thanks to my wonderful girlfriend Andrea Mitchell for her love and support and for putting up with lost weekends and odd working hours throughout this thesis

Table of Contents

Certificate of Examination ii
Abstract iii
Acknowledgements iv
Table of Contents v
List of Figures vii
List of Tables ix
List of Abbreviations x
1.0 INTRODUCTION 1
2.0 BACKGROUND AND LITERATURE REVIEW 5
2.1 Tissue Engineering 5
2.1.1 A New Generation of Biomaterials 5
2.1.2 Biomimetic Material Design Criteria 7
2.2 Electrospinning 11
2.2.1 History 11
2.2.2 Fundamentals 13
2.2.3 Parameters 17
2.2.3.1 Electric Field Strength 18
2.2.3.2 Polymer Solution Flow Rate 19
2.2.3.3 Concentration and Conductivity 19
2.2.3.4 Distance Between Needle-Tip and Collector 20
2.2.3.5 Ambient Parameters 21
2.2.4 Fiber Orientation and Alignment 21
2.2.5 Coaxial Electrospinning 23
2.3 Polymeric Devices for Protein Delivery 27
2.3.1 Controlled Release 27
2.3.2 Release Mechanism and Kinetics 35
2.4 Material Selection 39
2.4.1 Poly (ε-Caprolactone) 39
2.4.2 Trifluoroethanol 40
2.4.3 Poly (ethylene glycol) 41
2.4.4 Bovine Serum Albumin 41
2.4.5 PDGF-BB 42
2.4.6 TGF-β1 43
2.4.7 Radial Arterial Cells 44

3.0 METHODS AND MATEIALS **45**
3.1 Coaxial Electrospinning Apparatus **45**
3.1.1 Design 45
3.1.2 Parameters 47
3.2 Materials **48**
3.2.1 Shell Polymer Solution 48
3.2.2 Core Polymer Solution 49
3.2.2.1 Bovine Serum Albumin 49
3.2.2.2 Poly (ethylene glycol) 50
3.2.2.3 PDGF-BB 50
3.2.2.4 TGF-β1 50
3.3 Scaffold Characterization **51**
3.3.1 Scanning Electron Microscopy 51
3.3.2 Laser Scanning Confocal Microscopy 51
3.3.3 In Vitro Protein Release 52
3.3.3.1 Fluorescence Spectroscopy 52
3.3.3.2 Bradford Protein Assay 52
3.4 Cell Culture **54**
3.4.1 Cell Isolation and Culture 54
3.4.2 Cell Proliferation 56
4.0 RESULTS AND DISCUSSION **57**
4.1 Optimizing Flow Rates **57**
4.2 Scaffold Morphology **60**
4.3 Protein Loading **67**
4.4 Protein Release **70**
4.5 Cell Culture **82**
4.5.1 Proliferation 82
4.5.2 Morphology and Migration 85
5.0 CONCLUSIONS AND FUTURE WORK **91**
6.0 REFERENCES **95**
Appendix A **102**
Appendix B **103**
Curriculum Vitae **105**

List of Figures

Figure 1. Illustration of the systematic activation of a generic gene by a growth factor 9

Figure 2. Schematic illustration of the basic setup for electrospinning 14

Figure 3. Photographs displaying typical whipping instability of fibers during electrospinning 16

Figure 4. SEM images of aligned nanofibers [A-C] and nanotubes [D] of various materials 22

Figure 5. Schematic illustration and optical image of the parallel plate fiber collection method 23

Figure 6. Schematic illustration of the basic setup for coaxial electrospinning 24

Figure 7. Morphology of composite core-shell electrospun fibers subsequent to axial stretching. 26

Figure 8. BSA release from core-shell structured nanofibers I 30

Figure 9. BSA release from core-shell structured nanofibers II 31

Figure 10. Release profiles of gentamycin sulfate (GS) and resveratrol (RT) from coaxial PCL fibers. 32

Figure 11. Comparison between release profiles of PCL+BSA blend and PCL/BSA coaxial fibers 33

Figure 12. Release of BSA from coaxial PCL and various PEG/PCL blend nanofibers. 34

Figure 13 Chemical structure and ring opening polymerization of PCL 39

Figure 14. Chemical Structure of TFE 40

Figure 15. Digital photograph of the coaxial electrospinning setup in the lab 47

Figure 16. Digital photograph of coaxially electrospun PCL-BSA on glass slide after electrospinning 60

Figure 17. SEM of PCL-BSA coaxial scaffolds formed using a shell flow rate of 0.9 ml/hr and a core flow rate of 0.1 ml/hr [A,B], 0.2 ml/hr [C,D] or 0.3 ml/hr [E,F] 62

Figure 18. SEM of PCL-BSA coaxial scaffolds formed using a shell flow rate of 0.4 ml/hr and a core flow rate of 0.1 ml/hr [A,B], 0.2 ml/hr [C,D] or 0.3 ml/hr [E,F] 63

Figure 19. SEM of PCL-BSA coaxial scaffolds formed using a shell flow rate of 0.6 ml/hr and a core flow rate of 0.1 ml/hr [A,B], 0.2 ml/hr [C,D] or 0.3 ml/hr [E,F] 64

Figure 20. Histograms of fiber diameters for scaffolds formed using various parameters 65

Figure 21. Fiber diameters for scaffolds formed using various core and shell flow rates, showing the dependence of various flow rate combinations on fiber diameter (Mean ± standard deviation) 67

Figure 22. Confocal microscopy images of coaxial PCL scaffolds containing BSA-FITC..... 68

Figure 23. Confocal microscopy images of coaxial PCL/BSA-FITC scaffolds created using a shell flow rate of 0.6ml/hr and a core flow rate of 0.1 ml/hr [A,B], 0.2 ml/hr [C,D] or 0.3 ml/hr [E,F]..... 69

Figure 24. Cumulative release of BSA-FITC from coaxial PCL scaffolds (Mean ± standard deviation) 70

Figure 25. Square-root time plot of BSA-FITC release from coaxial PCL (shell flow rate = 0.6 ml/hr). 71

Figure 26. Amount of BSA released from coaxial PCL scaffolds formed using shell flow rate of 0.6ml/hr and various core flow rates shown (Mean ± standard deviation)..... 73

Figure 27. Fractional release of BSA from coaxial PCL fibers formed using a shell flow rate of 0.6ml/hr and various core flow rates shown (Mean ± standard deviation)..... 74

Figure 28. Square-root time plot of BSA release from coaxial PCL (shell flow rate = 0.6 ml/hr). 75

Figure 29. Amount of BSA released from coaxial PCL scaffolds formed using a shell flow rate of 0.4ml/hr and various core flow rates shown (Mean ± standard deviation)..... 76

Figure 30. Fractional release of BSA from coaxial PCL scaffolds formed using a shell flow rate of 0.4ml/hr and various core flow rates shown (Mean ± standard deviation)..... 77

Figure 31. Square-root time plot of BSA release from coaxial PCL (shell flow rate = 0.4 ml/hr) 78

Figure 32. Proliferation of RA cells in the presence of TGF-β1 release or PDGF-BB release compared to inert PCL control after being cultured for 24, 48 or 72 hours..... 83

Figure 33. Proliferation of RA cells cultured on PCL scaffolds releasing TGF-β1 or PDGF-BB compared to those cultured on inert PCL scaffolds after 24, 48 or 72 hours (Mean ± standard error)..... 85

Figure 34. Confocal microscopy images of RA cells cultured on inert PCL scaffolds [A,B] compared to those cultured on coaxial PCL scaffolds releasing TGF-β1 [C,D] or PDGF-BB [E,F] after 48 hours..... 86

Figure 35. Confocal microscopy images of RA cells migrating within the 3D fibers of scaffolds releasing TGF-β1 [A-C] or PDGF-BB [D-F] after 48 hours of cell culture 87

Figure 36. Confocal microscopy images of RA cells adhering to individual fibers of coaxial PCL scaffolds releasing PDGF-BB after 48 hours of cell culture..... 89

Figure 37. Confocal microscopy images of RA cells reaching confluency on scaffolds releasing TGF-β1 [A] and PDGF-BB [B] after 72 hours of culture 89

List of Tables

Table 1. Coaxial electrospinning parameters used for fiber optimization experiments 48

Table 2. Cell culture layout for RA cells seeded on scaffolds releasing PDGF-BB 55

Table 3. Cell culture layout for RA cells seeded on scaffolds releasing TGF-β1 55

Table 4. Flow rate dependence chart showing the effect of varying the core and shell flow rate to obtain [S] Spraying [D] Dripping or [F] Fibers 59

Table 5. Average fiber diameter of coaxial PCL/BSA scaffolds formed using various core and shell electrospinning flow rates (Mean ± standard deviation) 66

Table 6. Protein release efficacy from PCL/BSA scaffolds formed using the various parameters shown. 79

Table 7. RA cell counts after 24, 48 or 72 hours of culture on the various scaffolds 84

List of Abbreviations

3D	Three Dimensional
BMP-2	Bone Morphogenetic Protein-2
BSA	Bovine Serum Albumin
DNA	Deoxyribonucleic Acid
ECM	Extracellular Matrix
ELISA	Enzyme-Linked Immunosorbant Assay
FGF	Fibroblast Growth Factor
FITC	Fluorescein-isothiocyanate
GAG	Glycosaminoglycans
HBSS	Hank's Buffered Salt Solution
LSCM	Laser Scanning Confocal Microscopy
mRNA	messenger Ribonucleic Acid
NGF	Nerve Growth Factor
PCL	Poly (ε-caprolactone)
PDGF	Platelet Derived Growth Factor
PEG	Poly (ethylene-glycol)
PLA	Poly (lactic-acid)
PLGA	Poly (lactide-co-glycolide)
PLLA	Poly (L-lactide)
PPX	Poly(p-xylylene)
PVA	Poly (vinyl-alcohol)
RA	Radial Arterial
RT-PCR	Reverse Transcription Polymerase Chain Reaction
SEM	Scanning Electron Microscopy
TFE	Trifluoroethanol
TGF	Transforming Growth Factor
VEGF	Vascular Endothelial Growth Factor

Chapter One

1.0 Introduction

The failure of an organ or tissue is among the most frequent, devastating and costly problems in human health care. Due to limitations of conventional reconstructive materials and poor availability of donor tissues, tissue engineering has become a promising alternative. Tissue engineering applies principles of biology and engineering to the development of functional tissue substitutes, which hold great promise in restoring and maintaining tissue and organ function.

Most tissue engineering approaches make use of a biodegradable biomaterial forming a three-dimensional (3D) structure, or scaffold, which serves as an active analogue of the natural extracellular matrix (ECM). The scaffold promotes cell function by replacing the natural matrix until host cells can repopulate and synthesize a new natural ECM under suitable *in vitro* and *in vivo* conditions. To engineer functional tissue and to fulfill the required biological functions, morphological similarity to the native ECM environment is essential. This environment can be controlled through the localized and targeted delivery of tissue inductive factors from the scaffold to regulate pragmatic cellular events involved in tissue development.

Tissue engineering strategies often include signaling molecules, which attempt to reproduce the natural sequence of signal guidance involved in spontaneous tissue regeneration. Among the most fundamental signaling molecules involved in tissue regeneration are well-known proteins called growth factors. Growth factors are naturally occurring proteins that stimulate cell functions such as migration, proliferation, and differentiation. These signaling molecules are either cytokines or hormones that bind to specific cell membrane receptors. Cytokines are used in cell communication with autocrine, paracrine, endocrine and chemokine capabilities. Hormones are used in cell communication with endocrine and exocrine capabilities. The vital role of these growth factors as intricate signaling molecules cannot be overlooked within the process of tissue engineering.

In many early approaches, growth factors were simply dispersed into the cell-scaffold environment by including them into the growth medium used for cell culture. Since tissue regeneration depends on the localized delivery of specific proteins capable of providing biochemical cues, a random dissolution of growth factors into cell culture medium does not adequately mimic *in vivo* conditions. Furthermore, growth factors are very sensitive to their chemical environment and culture medium provides no protection from harmful molecules. Despite the development of the elemental process of tissue engineering, efforts to date have been largely empirical, due to the inadequate molecular cell-scaffold interface.

Over the last decade, this deficiency has become apparent and researchers have been directing their efforts to overcome current limitations with the controlled delivery of signaling molecules. A new trend of biomaterials for tissue engineering has emerged which is attempting to design an approach through which naturally occurring physiological mechanisms can be reproduced and carried out at a molecular level within the cell-scaffold interface [1-4]. The focus has begun to pull away from adding signaling molecules on a macro-scale and is moving towards the development of scaffolds that better mimic the temporal and spatial complexity seen *in vivo*. The ability to reproduce cell-signaling cues to control cell behavior has become the focus, where proteins could be functionalized within scaffolds and released in response to specific cell-mediated stimuli. This, in turn, would generate a highly regulated network of signals, able to selectively orchestrate the requirements of a fully functionalized tissue.

A scaffold capable of controlled delivery of growth factors or other soluble biochemical agents offers clear advantages over traditional practices of biological signal integration. The release rate of the signaling molecules can be regulated through various methods, while protecting the sensitive molecules from deactivation and denaturation. These methods will be outlined in the following chapters. The versatility of this novel tissue engineering platform satisfies the need of eliciting spatial and temporal control over morphogenic cues within the 3D scaffold environment. Recent developments have been very encouraging and have essentially laid the groundwork for a new generation of biomaterials.

The current study aims to develop a better understanding of the kinetics and characteristics of growth factor release from a biocompatible polymeric system while generating an optimization strategy for the formation and development of scaffolds with temporally and spatially controlled release. In addition, the scaffolds were used to study the influence of independently releasing two specific growth factors into the local microenvironment of cultured radial arterial (RA) cells.

Chapter Two

2.0 Background and Literature Review

2.1 Tissue Engineering

2.1.1 A New Generation of Biomaterials

The use of inert scaffolds has yet to generate promising results in tissue engineering applications. As a result, a new generation of biomaterials has recently emerged and is quickly reforming the process of tissue engineering. This new breed of biomaterials includes 3D scaffolds capable of mimicking the regulatory mechanisms of the ECM in natural tissue [2]. Although these novel scaffolds provide enhanced cell-scaffold interaction mechanisms, they provide an oversimplified representation of the natural ECM and fail to fully reproduce the spatial and temporal complexities seen in natural tissue. Through the development of these novel biomaterials, the symbiosis of materials engineering and molecular cell biology has not been applied to its full potential. Nevertheless, current research continues to explore and optimize the development of biomimetic nanofibers for storage and release of bioactive molecules. Preliminary work with electrospun bioactive fibers demonstrates the feasibility of such a dynamic system and results to date have been very encouraging, as is briefly highlighted in the following examples.

In an effort to mimic bone ECM, Li *et al* prepared silk fibroin fiber scaffolds containing Bone Morphogenetic Protein-2 (BMP-2) growth factor and nanoparticles of hydroxyapatite [5]. BMP-2 is well known as a morphogen to induce osteogenesis from stem cells. Silks are attractive biomaterials for bone tissue engineering because of their biocompatibility, slow degradability and superior mechanical properties. These silk-BMP-2 scaffolds supported higher calcium deposition and enhanced up-regulation of BMP-2 transcript levels of bone-specific markers compared to controls.

To address the issue of endothelial cell attachment in artificial vascularization, Williamson *et al* incorporated a model macromolecule into wet-spun Poly (ε-caprolactone) (PCL) fibers to investigate the potential of loading proteins [6]. Trypsin was successfully loaded into the fibers and had definitive release over a 48-hour period.

Casper *et al* prepared biologically active functionalized scaffolds to permit immobilization and long-term delivery of growth factors by incorporating heparin into electrospun nanofibers [7]. Heparin primarily serves to immobilize growth factors but is also known to control their mitogenic activity. It often serves as a cofactor to promote binding of growth factors to their receptors. The incorporation of heparin into an electrospun scaffold allows for exploitation of its natural affinity for growth factors as a strategy to deliver them directly to the biomimetic scaffold. The heparin was retained in the fiber for up to 14 days and improved the binding of fibroblast growth factor (FGF).

These results have been very promising. However, there is a further need to enhance the controlled delivery of bioactive molecules from polymeric systems and to exceed current delivery capabilities. Due to the bulk entrapment of the bioactive molecules in the previous examples, release is less controllable as the continuity and uniformity of the protein cannot be guaranteed. Furthermore, release of the protein is dependent on multivariable factors as the protein is randomly dispersed in the scaffolds.

Recently, groups have begun to take a closer look at tailoring the physical and morphological properties of scaffolds in an effort to further control the release of potent macromolecules into the local environment [8].

2.1.2 Biomimetic Material Design Criteria

Over the last several years, there has been a significant shift in the design criteria for biomaterials used in tissue regeneration. Tissue engineering constructs now contain a full integration of molecular cues to signal specific aspects of cell function. The dynamic relationship between cells and the natural ECM has been studied extensively for many years in an effort to exploit their properties and improve the mimicry seen in modern scaffold design. Ideally, such sophisticated properties embedded into scaffolds would allow the scaffolds to take an active role in secreting the cytokines and hormones required for various pathways of tissue development.

In the natural ECM environment, growth factors are essentially deposited within the fibrous network and released to the cells in the surrounding tissue in response to a wide array of physiological processes. Through the course of tissue development, suitable mass transport between cells and the engineered scaffold is required in order to meet the metabolic requirements of the cells. Tissue engineering often relies on the transplantation of cells onto a polymeric scaffold. During tissue engineering, diffusion of molecules within the cell culture medium is not sufficient to satisfy the high metabolic demand of the transplanted cells. Improved formation of engineered tissue can likely be achieved by the localized and controlled delivery of molecules which induce phonotypic and genotypic effects necessary to maintain and stimulate the cell population. Ideally, the delivery of growth factors from a polymer matrix would promote tissue formation.

In order to understand how cells will behave on a biomimetic scaffold, it is important to define the mechanisms by which they communicate in a physiological setting. Cells interact *in vivo* by releasing chemical messengers targeted towards other cells. These targeted cells may or may not be immediately adjacent to the signaling cell. The signaling cell secretes local regulators called paracrines to influence cells within the local vicinity and endocrines to influence more distant cells.

Growth factors are one class of local regulators. These cytokines are able to communicate with neighboring cells or distant cells depending on the desired effect. They bind to specific cell membrane receptors in order to trigger a cascade of regulatory events,

mediating cell function through activation and de-activation of cellular proteins. Many cells can simultaneously receive and respond to growth factors produced by a single cell in their vicinity. Growth factors play a pivotal role in normal tissue development and therefore must be present in a suitable fashion in the extracellular environment for the growth and development of engineered tissue [9-12].

The process by which a signal on a cell surface is converted into a specific cellular response depends on a series of steps called a signal transduction pathway, as shown in Figure 1.

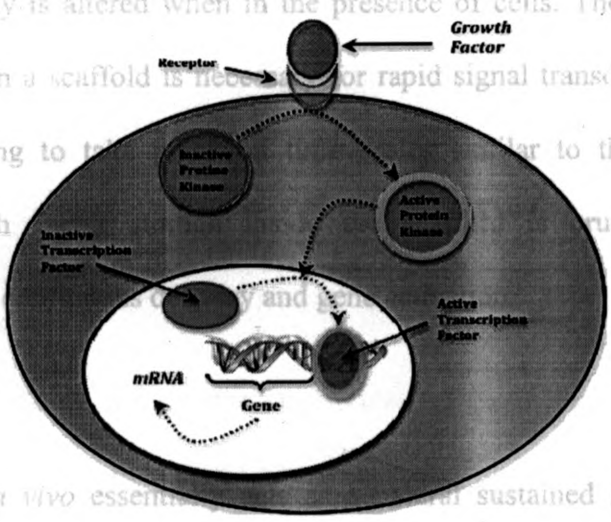

Figure 1. Illustration of the systematic activation of a generic gene by a growth factor

This illustration is a simplified representation of a typical signaling pathway leading to the regulation of gene activity in the cell nucleus. The initial signaling molecule, a growth factor, triggers a phosphorylation cascade in the cytoplasm, in which ATP molecules serve as sources of phosphate (not shown). The kinase protein enters the nucleus and

activates a gene regulating protein called a transcription factor. This protein, in turn, stimulates a specific gene to be transcribed into mRNA, which then mediates the synthesis of a specific protein.

The proteins created by this pathway ultimately lead to the regulation of one or more cellular functions. Most molecular messengers that produce gene regulation responses, including growth factors, are synthesized as membrane-bound precursors that must be modified to be released in the active form. They are often bound to ECM molecules, such as Glycosaminoglycans (GAGs) (e.g. heparin). By interacting with these molecules, growth factor activity is altered when in the presence of cells. The inclusion of active growth factors within a scaffold is necessary for rapid signal transduction, allowing the extracellular signaling to take place on time scales similar to that inside the cells. Furthermore, growth factor storage inside the scaffold is crucial to maintaining homeostasis through continuous delivery and gene activation.

The natural ECM *in vivo* essentially acts as a natural sustained release reservoir for growth factors. This form of release is fundamental to stimulating the repair processes during natural tissue regeneration, which takes extended periods of time to be carried out. The traditional method of providing these crucial signaling proteins to tissue development *in vitro* has been to add them to tissue culture medium. Nevertheless, this procedure has been relatively unsuccessful and the translation of this concept *in vivo* is virtually impossible. For example, Cao *et al* recently attempted an intracoronary and intravenous

infusion of VEGF and FGF to assist in tissue development, with unsuccessful results [11].

Growth factor localization is required in order to confine the activity and to avoid exposure of these potent proteins to non-target sites. This presents a clear conviction that a tissue engineering scaffold should be inspired by reproducing the natural occurrence of signaling molecules and by maintaining the spatial and temporal presentation of these proteins *in vitro*. As a result, this issue has become a key component to the design criteria of tissue engineering scaffolds and has led to a surge of research in order to develop complex polymer-based protein delivery systems [2, 8].

2.2 Electrospinning

2.2.1 History

Electrostatic fiber spinning (electrospinning) traces its roots back to the early 1930's when it was used to fabricate industrial or household non-woven fabric products. In 1934, Formhals published a patent describing an experimental setup for the production of polymer filaments using an electrostatic force [13]. A polymer solution was introduced into an electric field between two electrodes bearing electrical charges of opposite polarity. One of the electrodes was placed in the solution and the other was placed onto a collecting plate. A polymer filament was formed between the electrodes as the solution evaporated leaving the fibrous polymer on the collecting plate. Although the fibers

produced by Formhals were much larger than the nanofibrous structures of interest in today's technological applications, his work set the stage for a new generation of fiber processing.

Throughout the 1950's, several variations of the electrospinning process were experimented using solutions ejected from a glass capillary [14, 15]. In 1966, Simons patented an apparatus for the production of non-woven, ultra thin, light weight fabrics using electrospinning [16]. In 1969, Taylor did a study of the polymer droplet at the tip of the capillary in a typical electrospinning setup [17]. He quantified the mechanical instabilities and from this the term 'Taylor cone' was coined for the shape derived by the forces on the liquid jet as it left the capillary. This study led to a better understanding of the process by which the polymer solution streams from the needle. In 1971, Baumgarten developed an electropsinning apparatus capable of fabricating acrylic fibers with diameters in the range of 50–1,100 nm, leading to the conception of electrospun nanofibers [18].

In 1987, Hayati *et al* studied the experimental conditions and factors causing highly conductive fluids exposed to increasing electric fields to produce unstable streams [19]. Finally, in 1995, Doshi and Reneker investigated how changing the polymer concentration of the solution and the applied voltage affect the nanofiber formation [20]. As can be seen by a simple historical account of this infant technology, the

electrospinning process has essentially remained the same as that described by Baumgarten in the 1970's.

Although the concept of electrospinning can be traced back to the early 1930's, the term electrospinning was coined by several research groups in 1994 as a revived interest in this technique developed due in part to a surging interest in nanotechnology material development. Throughout the past decade, electrospinning has gained remarkable popularity due to its simplicity and its ability to generate a high throughput of true non-woven fibers with high uniformity and continuity.

2.2.2 Fundamentals

The electrospinning process is based on the uniaxial stretching of a viscoelastic jet derived from a polymer solution. Fibers of nanoscale diameter are generated because elongation is accomplished by a contact-less scheme in which friction is negligible through the application of an external electric field. Moreover, electrospinning is a continuous process generating high continuity uniform fibers over an extended time period and therefore is suitable for high-volume production.

There are only a few components necessary to fulfill the requirements of electrospinning. In brief, a polymer solution is loaded into a syringe and this viscous liquid is driven to the needle tip using a syringe pump, forming a meniscus at the tip. An electrode is placed on

the needle and another electrode, of opposite polarity, is attached to a collecting plate. A DC voltage is applied between the needle and grounded collecting plate, forming an electric field, which stretches the droplet into an unstable electrified jet. The high electric field (10-30 kV) causes instability between the surface tension of the droplet at the needle tip and the electrostatic force on the suspended droplet. The electric field induces a positive charge on the surface of the spinning solution at the needle tip. Mutual charge repulsion and the contraction of the surface charges to the counter electrode cause a force directly opposite to the surface tension [21]. A schematic illustration of the experimental setup is shown in Figure 2 [22]. As the electric field is intensified, the hemispherical surface of the spinning solution at the needle tip elongates to form a conical shaped jet, termed the Taylor cone [17]. The cone is subsequently elongated into a stable jet, which forms the initial stage of nanofiber formation.

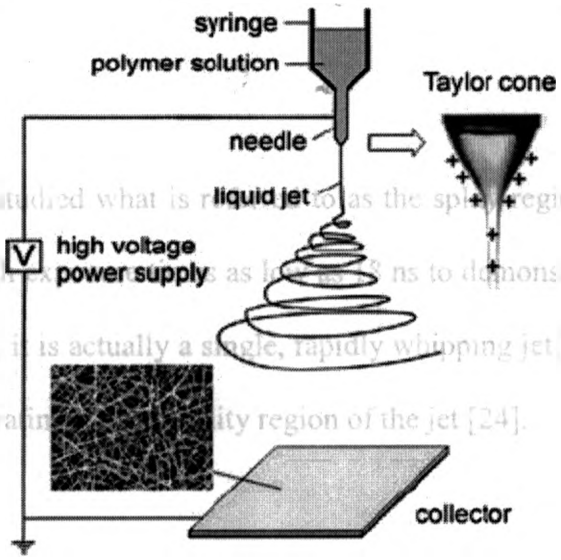

Figure 2. Schematic illustration of the basic setup for electrospinning. This figure was reproduced from [22] with permission. Copyright Wiley-VCH Verlag GmbH & Co, 2004

This stable jet was described in substantial detail by Reneker and Chun as having four essential components: the base, the jet, the splay and the collection [23]. As the polymer solution jet is discharged from the needle tip in the base region, it manifests itself as a Taylor cone, which is indicative of proper fiber extrusion. The shape of this base region depends on the force of the electric field and the surface tension of the spinning solution. If the electric field is strong enough, a jet will be ejected from the surface, even if the meniscus is essentially planar. The jet is charged in the base region and spinning solutions with higher conductivity are most favorable for jet formation [18]. Following the base region, electric forces accelerate and stretch the polymer jet, causing the diameter to decrease and the length to increase. Solvents with high vapor pressures may begin to evaporate, causing an additional decrease in polymer jet diameter. Prior to 2001, it was believed that during evaporation of the solvent, the fiber would splay into a series of individual fibers that would continue to be drawn towards the collector in a random fashion [18].

Shin *et al* have since studied what is referred to as the splay region and have used high speed photography with exposure times as low as 18 ns to demonstrate that, where the jet appears to be splaying, it is actually a single, rapidly whipping jet [24]. Figure 3 contains two photographs illustrating the instability region of the jet [24].

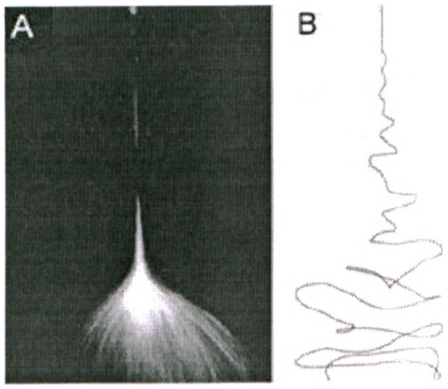

Figure 3. Photographs displaying the solution jets during electrospinning using capture times of [A] 1/250 s (vertical distance = 20cm) and [B] 18 ns (vertical distance = 9 cm) showing the typical whipping instability of fibers. These two figures were adapted from [24] with permission. Copyright Elsevier Science, 2001

It has been shown that after traveling a short distance through a high electric field, the jet becomes unstable, begins to whip with a very high frequency, and undergoes bending and stretching [19]. The behavior of the jet has been modeled in terms of three instabilities: the classical Rayleigh instability and two "conducting" instabilities. Surface tension dominates the axisymmetric Rayleigh instability and this effect is reduced in high electric fields or charge densities [19]. Electric forces dominate the conducting modes, which are independent of surface tension. One conducting mode is axisymmetric and the other is nonaxisymmetric. The latter mode accounts for the observed whipping instability in the polymer jet. Hayati *et al* compared these instabilities using various electrospinning parameters and outlined the conditions under which whipping was expected [19]. These predictions agreed well with experimental results.

Before electrospinning can take place, polymers must be dissolved in an appropriate solvent capable of generating a homogeneous solution. When the solid polymer is

dissolved entirely in a proper amount of appropriate solvent, it becomes a fluid form referred to as a polymer solution. Before reaching the collecting plate, the solvent evaporates and the fiber becomes essentially solidified. The jet is then collected as a non woven mat of dry nanoscale fibers.

2.2.3 Parameters

The electrospinning process is very sensitive to manipulation and can be easily modified using a number of important parameters. The parameters can be classified in terms of process variables, solution properties and ambient parameters. The process variables include the electric potential at needle tip, the distance between needle tip and collecting plate, the solution flow rate, the needle tip design and the collector geometry. The solution properties include viscosity, conductivity, polymer molecular weight, dipole moment, dielectric constant and surface tension. It is important to note that the effects of these parameters can be difficult to isolate due to the profound interrelationship between many of the parameters. For example, changing the distance between the needle tip and collecting plate can change the relative electric field strength and changing the solutions concentration can change its viscosity. The ambient parameters include temperature, humidity, and gases in the electrospinning chamber.

Although many distinct polymers have been electrospun, it is difficult to use a systematic investigation of conditions and parameters to predict optimal spinning for all polymers. Generally, a trial and error approach has been employed, in which the spinning

parameters are manipulated until uniform fibers are obtained. During any systematic investigation of electrospinning parameters, it is important to define the ultimate goal of this technology as certain requirements can only be met by identifying specific needs of the final product. Accordingly, electrospinning aims to fabricate nanofibers with ideal targets such as consistent and controllable diameter and minimal to no defects or impurities, with a non-woven single fiber collection. As such, the various parameters involved can heavily influence the transformation of polymer solutions into nanofibrous structures and will be explored in detail.

2.2.3.1 Electric Field Strength

Among all of the controlled variables discussed here, the effect of the electric field strength on fiber morphology has received the most attention within the research community. An electric field that is too weak will result in no fiber formation as the field strength is simply insufficient to overcome surface tension of the suspended droplet. When a moderate electric field is used, the solution drop suspended at the needle tip develops into a Taylor cone and a jet emerges producing a uniform fiber, assuming the surface tension is overcome by the electric field. When the electric field is increased, the meniscus at the needle tip decreases in volume and becomes less rounded. This causes the Taylor cone to recede so the liquid jet develops much closer to the tip and beading is often observed in the collected fiber [25]. Further increasing the electric field has been shown to cause the liquid jet to move around at the needle tip forming no Taylor cone.

2.2.3.2 Polymer Solution Flow Rate

Few studies have investigated the systematic relationship between solution flow rate and fiber morphology, however, consistent observations have been made by many groups and these trends appear to have remarkable reproducibility. In general, it has been found that lower flow rates yield fibers with decreased diameters [26]. Flow rates that are too high have been found to generate beading within fibers because the solvent does not have time to fully evaporate before the fiber reaches the collecting plate and this phenomenon has been shown repeatedly by various groups [27].

2.2.3.3 Concentration and Conductivity

The viscosity of the polymer solution can be manipulated by varying the polymer concentration. This parameter has been found to be one of the most influential factors of fiber size and morphology. At low polymer concentrations, beading has been shown to consistently occur and the process under these conditions is more characteristic of a similar technology known as electrospraying [28]. Junctions and bundles have also been observed in these low concentration polymer fibers, indicating that the solvent did not entirely evaporate prior to reaching the collecting plate. At higher polymer concentrations, uniform fibers with few beads and junctions are generated. Solutions containing a polymer concentration that is too high result in inconsistent fiber formation and in some cases no fiber at all. If the solution is too viscous, the droplet simply dries out at the needle tip before a jet is initiated and electrospinning does not occur.

Increasing the polymer solution conductivity can be achieved through the independent addition of salts and alcohol. It has been shown that increasing the conductivity can generate smoother, more uniform fibers with less beading [29, 30]. Accordingly, the addition of cationic surfactants has been shown to prevent beading whereas the addition of nonionic surfactants has not been shown to prevent beading. This being the case, it has been hypothesized that charged surfactants increase solution conductivity, causing an increase in the whipping instability yielding more uniform fibers [31].

2.2.3.4 Distance Between Needle Tip and Collector

The distance between the needle tip and collecting plate has been investigated experimentally as a way to control fiber diameter and morphology. Various distances have been examined and it has been shown that a minimum distance is required to allow sufficient evaporation of solute before the fibers reach the collector [32]. If the distance is too large or too small, beading has been shown to occur, indicating that there exists a relatively narrow range within which fiber morphology can be optimized. It has been observed that the optimum distance is highly dependant on the specific polymer solution used [33]. Using some polymers, such as PVA and chitosan, varying the distance produces no significant effect on fiber morphology. In contrast, when certain polymer solutions are used, decreasing the distance correlates to a decrease in fiber diameter. Therefore, there is no definitive universal effect of the distance between the needle tip and collector on fiber morphology, however, there do exist some clear correlations when using certain specific polymer solutions.

2.2.3.5 Ambient Parameters

Very few studies have investigated the effect of ambient conditions on fiber morphology. One study involved a systematic investigation of the effect of temperature on fiber diameter [34]. It was found that increased temperatures generate fibers with decreased fiber diameter. This decline in diameter was simply attributed to the decrease in viscosity of the polymer solution at increased temperatures. A separate study involved varying the ambient humidity and its effect on fiber morphology [35]. It was found that increasing the humidity generated fibers with small circular pores on their surface.

2.2.4 Fiber Orientation and Alignment

Alignment of electrospun nanofibers is a difficult task because the polymer jet trajectory is in a complex 3D "whipping" form, rather than in a straight line. The nanofibers typically obtained are in a random non-woven mesh-like form, which are useful in certain applications, however, fiber alignment is equally desirable for various applications. A number of techniques have been explored in order to align electrospun nanofibers, two of which have been very successful.

The first technique is known as the "rotating drum" method and involves rotating a cylindrical drum at thousands of revolutions per minute. The drum is grounded and acts in place of the traditional collecting plate. When a linear speed of the rotating cylinder surface matches that of the electrospun jet, the fibers are deposited on the surface and

orient circumferentially in a tightly aligned manner. Perfect alignment, as shown in figure 4, is difficult to achieve because it requires a specific alignment speed of the rotating drum and this speed is difficult to determine because polymer jets formed through electrospinning do not always have a consistent or predictable motion [36, 37].

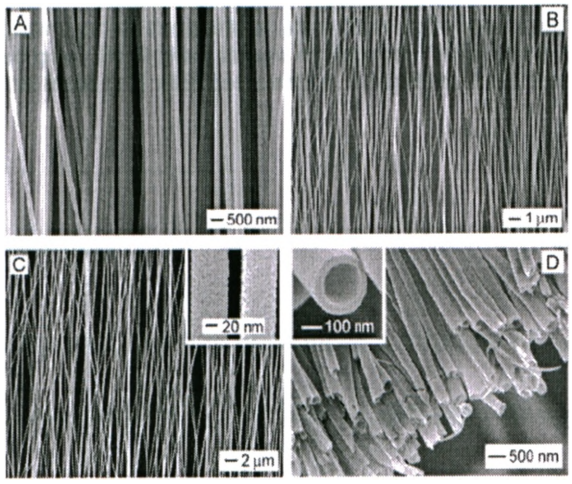

Figure 4. SEM images of aligned nanofibers [A-C] and nanotubes [D] of various materials: [A] Carbon [B] TiO2 / PVP [C] SnO2 and [D] Anatase. These figures were adapted from [36,37] with permission. Copyright American Chemical Society, 2003, 2004

The second technique is known as the "parallel plate" method and involves a pair of split electrodes on the plane of the collecting plate surface. By placing two conductive strips in a parallel orientation on either side of the collecting plane, electrospun fibers can be aligned axially over relatively long length scales, up to several centimeters [37]. Figure 5 is illustrative of the precise alignment generated using this method.

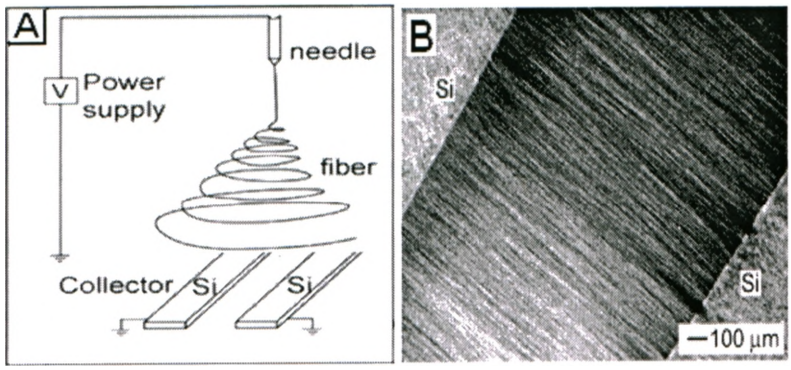

Figure 5. [A] Schematic illustration of the parallel plate fiber collection method using two conductive plates separated by a void gap. [B] Optical image of aligned PVP fibers collected across void gap. These figures were adapted from [37] with permission. Copyright American Chemical Society, 2003

2.2.5 Coaxial Electrospinning

The development of electrospinning has introduced a window of opportunity with respect to composite material development. A variety of different designs and configurations have been used to investigate ways of increasing throughput and developing composite materials through modification of the electrospinning needle tip. Various unique fabrication methods have been demonstrated for generating composite fibrous nanostructures such as phase separation [38], self assembly [39], template synthesis [40] and melt blowing [41]. However, among these, coaxial electrospinning seems to provide the simplest approach producing continuous fibers with uniform diameters capable of housing sensitive bioactive molecules.

Coaxial electrospinning is achieved using two independent feeds of polymer solutions where one capillary is inserted inside a slightly larger capillary and the polymer solutions flow through the needle tips simultaneously through a concentric orifice arrangement, as

shown in Figure 6. The coaxial electrospinning process is based on the uniaxial stretching of the two concentric viscoelastic jets derived from the two separate polymer solutions. The result is a core-shell fibrous structure consisting of two separate materials capable of independent functions.

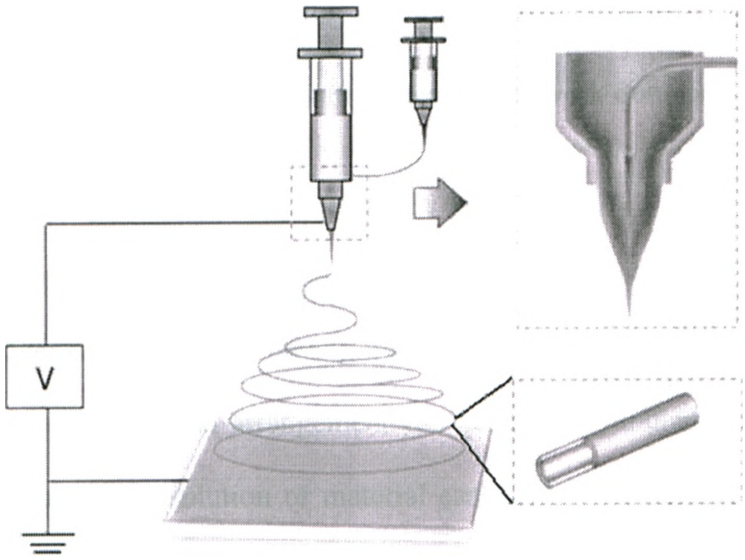

Figure 6. Schematic illustration of the basic setup for coaxial electrospinning

This technique has been used to fabricate hollow nanofibers and core-shell nanofibers capable of satisfying the requirements of various applications. Undesirable mixing of the separate polymer solutions with similar molecular properties can be prevented by the low diffusion coefficients of the individual polymers relative to the fast stretching and solvent evaporation taking place during the spinning process. The travel time of the jet in the air has been shown to be on the order of milliseconds, and therefore is far shorter than the time needed for significant diffusion-based spreading.

The characteristic time of bending instability in electrospinning is roughly 1 ms (t_1). The characteristic time of diffusion spreading of a sharp boundary between two different polymers due to their mutual diffusion is d^2/D_a (t_2), where d is the cross sectional diameter and D_a is the diffusion coefficient of the polymer solution [28]. Using an estimate of $d = 5x10^{-7}m$ and D_a in the range of 10^{-13} - 10^{-10} m^2/s, t_2 falls in the range of 10 - 1000 ms. Since t_2 is larger than t_1, the sharp boundaries should survive in the coaxial electrospinning process, in agreement with experimental work done previously [28].

Coaxial electrospinning is a very useful technique for the development of composites in which a heterogeneous structure having two independent functions is required. The novelty lies in that the coaxial arrangement can generate a tubular-shaped fiber on the outside while a functional solution or material can occupy the core. The thickness and diameter of the core and shell can be controlled by varying the electrospinning parameters within a range of determined values in order to optimize fiber morphology. Figure 7 reveals the morphology of coaxial fibers subjected to stretching [42].

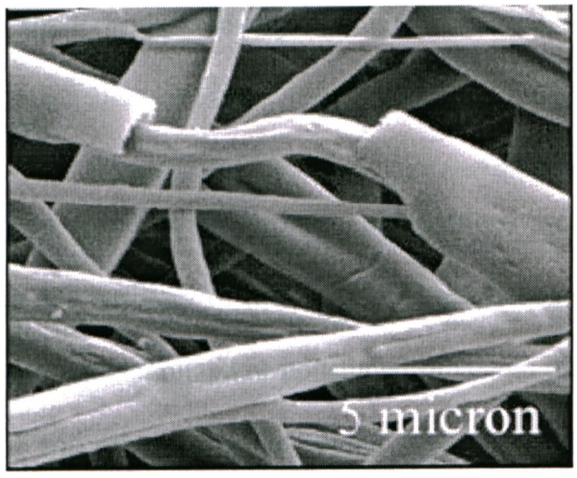

Figure 7. Morphology of composite core-shell electrospun fibers composed of zein protein as shell and PCL as core shown subsequent to axial stretching. This figure was reproduced from [42] with permission. Copyright Wiley-VCH Verlag GmbH & Co, 2007

By augmenting the intrinsic properties of specific polymers and proteins, an ideal material can be fabricated using this technique. For instance, the controlled delivery of drugs and pharmaceuticals in the most physiologically suitable fashion has always been an important concern within the biomedical community. By using the concept of coaxial electrospinning, a carrier material can be electrospun into a tubular structure within which proteins or other bioactive agents can be encapsulated. In either case, molecular release kinetics can be evaluated *in vitro* and systematically modified for optimal results by manipulating the various electrospinning parameters. It has been emphasized that such a process has a higher efficiency than traditional methods used for encapsulation of growth factors or proteins [43, 44]. Furthermore, coaxially electrospun fibers have received an increasing interest for their use as tissue engineering scaffolds [45]. These coaxial fibers have been shown to be cytocompatible using various composite material combinations including PCL [46].

2.3 Polymeric Devices for Protein Delivery

2.3.1 Controlled Release

As a large number of new proteins and protein combinations are being investigated for therapeutic applications, the delivery of these proteins has become an important area of research. Many proteins are metabolized or consumed *in vivo* at different rates, therefore, the delivery of proteins and other bioactive agents in the most physiologically suitable fashion is an important concern. In the past, multiple doses or injections have been required in order to achieve a desired therapeutic effect [2]. In an effort to improve the therapeutic efficiency, researchers have turned to the concept of controlled delivery through various technologies intended to mediate the release of these potent macromolecules *in vivo*.

In general, a high surface area to volume ratio and a small dimension of the particular protein results in better absorption and uptake by the recipient, be it an entire patient or merely a single set of cells. This is based on the simple principle that the dissolution rate of a protein increases with increasing surface area of both the protein and its respective carrier. Electrospun nanofibers for protein delivery have an additional advantage. Unlike common encapsulation methods involving complex preparation and production, therapeutic compounds can be easily incorporated into their respective carrier polymers through electrospinning or coaxial electrospinning. As such, electrospun fibrous mats have been investigated for their potential use as support carriers for protein delivery [5-7, 43-45, 47-54].

The first study of this type took place in 2002, in which Kenawy *et al* demonstrated controlled release of a model drug blended into electrospun PLA fibers [55]. Soon after, Ignatious *et al* investigated electrospun polymer nanofibers for pharmaceutical applications, which could be designed to provide rapid, immediate, delayed or modified release [56]. In another report, Kim *et al* developed biodegradable nanofibers of PLA loaded with an antibiotic drug called Mefoxin [57]. The drug was released over a period of seven days without the loss of structural integrity or bioactivity.

Each of the reports referenced above used the process of simply mixing drugs and carrier polymers in the same solution before electrospinning. In this case, depending on the interactions between the drug and polymer carriers within the solution, likely interaction modes of the drugs with the resultant nanofibers are: (1) a blend of the drug and carrier polymer integrated into one single fiber entangled evenly at a molecular level due to good compatibility; (2) two electrospun nanofibers interlaced within one another, one being the drug and the other the carrier; and (3) tiny particles of the drug being attached to the surface of the nanofibrous carrier. The mechanisms in (2) and (3) are susceptible to problems associated with initial stage burst release, making them an inferior choice compared to mechanism (1).

It was recently reported that PVA nanofibers loaded with BSA were obtained through electrospinning [58]. These fibers were subsequently coated with PPX to significantly reduce the release rate of BSA over a 20-day period. Another study reported the release

of antibiotics from electrospun PLA nanofibers [59]. Luu *et al* prepared composite nanofibers consisting of PLGA and DNA by electrospinning to be used as a plasmid DNA delivery system for gene therapy [60].

Apart from the above-mentioned approaches, nanofibers encapsulating bioactive agents for controlled release can be fabricated through coaxial electrospinning. Using this technique, proteins can be released through the shell of the structure as long as the carrier polymer is permeable to the molecules or the molecules can be released over a sufficient time period as biological degradation of the polymer occurs. This core-shell structure is able to provide a protective barrier for certain sensitive bioactive molecules such as growth factors, which must be retained in an active state prior to their role in early stage wound healing or cell-scaffold stimulation in tissue engineering.

Although research in this highly technical field is still in its infancy, there have recently been several encouraging studies involving the coaxial electrospinning of biological macromolecules. The following examples are meant to provide a comprehensive analysis of the development and current status of coaxially electrospun PCL fibers housing proteins in a core-shell fibrous reservoir for various controlled release applications.

In 2005, PCL was first introduced as a means of encapsulating proteins for controlled release through coaxial electrospinning [44]. Jiang *et al* successfully encapsulated PEG

containing BSA at 40 mg/mL into the core of coaxial nanofibers with a PCL shell and demonstrated controlled release over an extended period of time, shown in Figure 8.

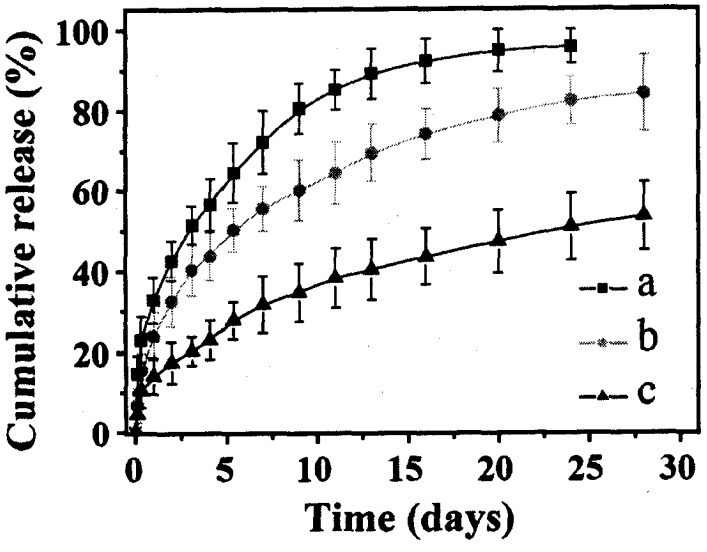

Figure 8. BSA release from core-shell structured nanofibers using a core flow rate of 2 [a] 1 [b] or 0.6 [c] ml/hr where the BSA loading in the fibers was 5.6%, 3.1% and 2.0% respectively. This figure was reproduced from [44] with permission. Copyright Elsevier Science, 2005

In 2006, the same group encapsulated a BSA core at 150 mg/mL into a PCL and PCL/PEG blend shell through coaxial electrospinning [61]. This study involved a systematic investigation of PEG as a means to control the BSA release rate by exploiting the phenomenon of phase separation between the PCL and PEG. It was discovered that BSA release could be modulated by both the loading concentration as well as the PEG fraction in the shell component, as shown in Figure 9. By increasing the BSA concentration and PEG fraction, an increase in BSA release was consistently shown.

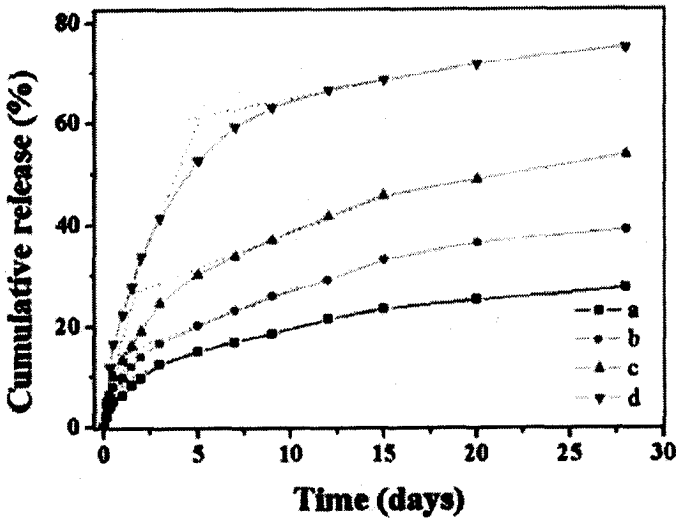

Figure 9. BSA release from core-shell structured nanofibers where the PEG/PCL fraction in the shell was [a] 0.4 [b] 0.2 [c] 0.1 and [d] 0.05. This figure was reproduced from [61] in accordance with the 'fair dealing' clause of the Canadian Copyright Act, provided by John Wiley and Sons, Ltd.

While there are clear benefits to the controlled delivery of bioactive proteins, there are also benefits to the controlled delivery of drugs for therapeutic applications. In 2006, Huang *et al* were the first to successfully coaxially electrospin two separate model drugs into the core of PCL nanofibers [43]. The group was interested in temporal protection of low molecular weight drugs, as they need to be sheltered from harsh environments for a period of time prior to their wound healing applications. Release profiles of the two separate drugs can be seen in Figure 10.

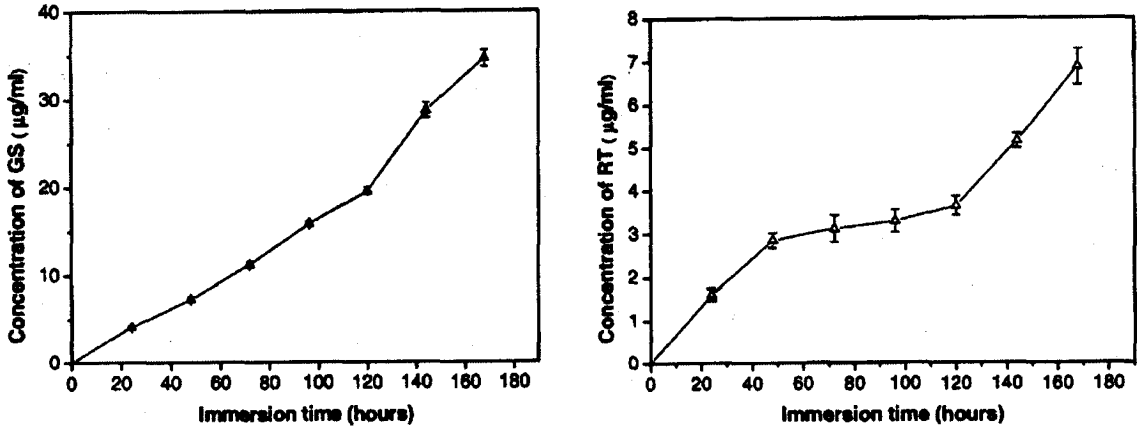

Figure 10. Release profiles of gentamycin sulfate (GS) and resveratrol (RT) from the core of coaxial fibers composed of a PCL shell. Samples were incubated in PBS containing lipase degradation molecule. This figure was reproduced from [43] in accordance with the 'fair dealing' clause of the Canadian Copyright Act, provided by John Wiley and Sons, Ltd.

It was found that drug release was smooth over a 7-day period, exhibiting no burst release and nearly zero-order release kinetics, suggesting a polymer degradation-based release. This theory was substantiated by the fact that there was a degradation molecule, *pseudomonas* lipase, included in the release medium.

In an effort to further tailor the coaxial electrospinning conditions used to encapsulate protein into PCL fibers, Zhang *et al* encapsulated BSA at 1 mg/mL within a PCL shell [49]. BSA loading showed two stages of release: an initial burst release followed by a constant linear release, as shown in Figure 11. This study was the first to suggest that the use of core-shell nanofibers may alleviate the initial burst release and improve the sustainability of nanofibrous protein release devices.

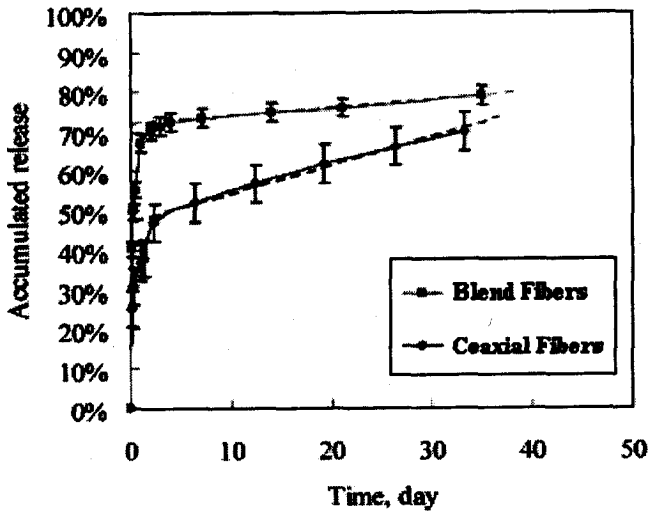

Figure 11. Comparison between release profiles of PCL+BSA blend and PCL/BSA coaxial fibers. The initial burst in coaxial fibers led to release amounts of approximately 45% over a 2-day period. This figure was reproduced from [49] with permission. Copyright American Chemical Society, 2006

The only investigation of growth factor release from coaxial electrospun PCL fibers found in the literature was performed in 2006 [45]. In an effort to provide biochemical signals to cultured fibroblasts, Liao *et al* studied the release of PDGF-BB (20μg per each 6mg scaffold) from coaxial fibers with a PCL/PEG blended shell. Incorporation of PEG was a means to form pores in the shell to aid in growth factor release. It was discovered that PEG leached out of the shell in a concentration and molecular weight-dependant fashion, leading to BSA release half lives ranging from 1-20 days, as shown in Figure 12.

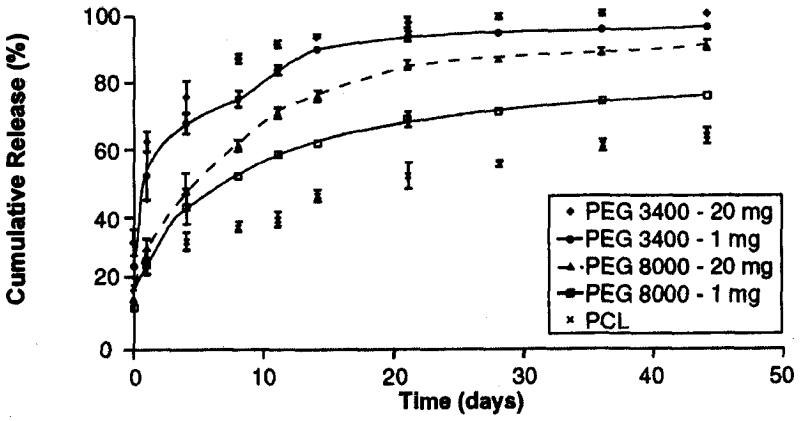

Figure 12. Release of BSA from coaxial PCL and various PEG/PCL blend nanofibers. This figure was reproduced from [45] with permission. Copyright Future Medicine, 2006

Optimized PDGF-BB encapsulated coaxial nanofibers were shown to completely release the protein with nearly zero order release kinetics and preserved bioactivity, as demonstrated by the proliferation of fibroblasts incubated in the presence of PDGF-BB released from the fibers. It is important to note that the cell culture studies were not performed on the coaxial scaffolds, but merely in the presence of the release buffer containing the released PDGF-BB.

Core-shell structured nanofibers are reservoir-type release devices. These devices have the advantage of providing a constant release rate over a substantial time period and have a higher loading level of bioactive agents than many other system [62]. The release rate from reservoir devices is critically dependent on shell thickness, surface area, permeability and defects such as pinholes in the fiber. Encapsulation with core-shell composite nanofibers provides high surface area for mass transfer, functionalization and protective function for preserving the bioactivity of encapsulated proteins.

2.3.2 Release Mechanism and Kinetics

The effective use of protein delivery scaffolds for tissue regeneration requires accurate control of protein release over the period of scaffold activity, in order to ensure release efficacy and to eliminate potential cytotoxic effects. The rate of protein release has been shown to vary greatly based on the polymer of the carrier as well as the protein being released [44, 45, 47, 49, 53, 55, 61, 63-65]. Therefore, tailoring the delivery of specific growth factors requires an understanding of the therapeutic cellular requirements and is achieved by carefully designing unique polymeric scaffold properties.

Controlling the rate of hydrophilic protein release is challenging when using hydrophilic polymers, as the matrix tends to swell in an aqueous environment and the protein is able to rapidly diffuse through swollen regions of the matrix. As a result, the use of hydrophobic polymeric carriers tends to be more suitable for the controlled delivery of hydrophilic proteins, providing a more stable carrier for the sensitive protein. PCL is ideal for the delivery of hydrophilic proteins since it is hydrophobic and has an inherently low level of swelling in aqueous environments [66].

Although the exact mechanism of protein release from electrospun PCL fibers has not been clearly demonstrated, several studies suggest that there are two predominant mechanisms: Diffusion [63] and porous dissolution [67]. The majority of studies involving coaxially electrospun PCL suggest both mechanisms as being present to

varying degrees over the course of the release experiments [44, 45, 49, 61]. If the diffusion rate is higher than the dissolution rate, diffusion will dominate and vice versa.

Chew *et al* investigated the incorporation of NGF into PCL fibers at a loading level of 8.3 μg/mL [53]. It was shown that the mass loss of PCL, over a release period of three months, was insignificant and that diffusion was the predominant release mechanism. In a similar study, rifampin was incorporated into PLLA fibers at various loading concentrations [47]. The PLLA was subsequently degraded by a degradation enzyme, proteinase K. In this case, the release kinetics were nearly zero-order and the drug was released at approximately 7% per hour, attributed mainly to the PLLA degradation.

When bioactive materials are encapsulated via coaxial electrospinning, the release mechanism is most frequently illustrated by two stages: an initial burst release followed by a more constant release profile. The initial burst release is likely related to dissolution of core material near the surface vicinity whereas the linear release is likely related to diffusion from the deeper regions of the core-shell structure.

Diffusion is commonly described using Fick's Laws by relating the diffusive flux (amount that flows through a unit area per unit time) to the concentration field, by postulating that the flux goes from regions of high concentration to regions of low concentration, with a magnitude that is proportional to the concentration gradient. In one

spatial dimension, this is: $J = -D(dc/dx)$. In this equation, D is the diffusion coefficient and is proportional to the velocity^2 of the diffusing particles, which depends on the temperature, viscosity of the fluid and the size of the particles according to the Stokes-Einstein relation (hydrodynamic diameter). For biological molecules the diffusion coefficients normally range from 10^{-11} to 10^{-10} m^2/s. Fick's second law involves the addition of a time domain to the first law to predict how diffusion causes the concentration field to change with time. It is derived from Ficks first law using a mass balance as follows: $(dc/dt) = -(d/dx)J = -(d/dx) \times -D(dc/dx) = D(d^2c/dx^2)$. In other words, as time passes while diffusion takes place, the concentration gradient slowly decreases, thus decreasing the flux and resulting in a non-linear release profile.

In 1987, Ritger *et al* developed an equation to describe the transport of drugs by Fickian diffusion through non-swellable devices: $M_t/M_\infty = kt^n$. Where M_∞ is the mass of drug released as time, t, approaches infinity, k is a constant that incorporates the characteristics of the polymer and drug and n is the diffusional exponent. According to Ritger, release by Fickian diffusion is defined by $n = 0.5$ and anomalous (non-Fickian) transport by $n > 0.5$. Furthermore, M_t/M_∞ is only applicable to 60% release to retain validity [50, 64]. This formula can be condensed to: $M_t/M_\infty \alpha t^n$. Furthermore, for Fickian diffusion, $n = 0.5$ and so the formula becomes: $M_t/M_\infty \alpha t^{0.5}$. In other words, in the case of Fickian diffusion, the initial 60% of cumulative release is proportional to the square root of time. This relationship is often used in the literature to identify diffusion-based release [44, 49, 61].

Since diffusion has repeatedly been proposed as the predominant release mechanism in polymer carrier protein delivery, a diffusion model is required to fully appreciate the process. Solid state-diffusion of small molecules from polymeric systems was studied by Li *et al* using molecular dynamics computer simulations [68]. The diffusion coefficients were predicted to be on the order of 10^{-6} to 10^{-4} cm^2/s. These values are several orders of magnitude larger than the values expected in solid-state diffusive release alone. This disagreement was attributed to an insufficient calculation of molecular forces. The discrepancy was demonstrated previously by Saltzman *et al*, who argued that pore interconnectivity and molecular dissolution may explain the low values of the effective diffusion coefficients and release of less than 100%, even at the end of very long experiments [69].

The ideal release mechanism in protein release systems is zero-order release, in which the release profile is linear and contains no initial burst release. This situation requires complete encapsulation of the protein with diffusion and polymer degradation at defined rates. Simple enzymatic degradation of PLLA electrospun fibers has been shown to follow zero-order release kinetics, in which drug release is correlated to degradation rate [70]. In most cases, some level of dissolution is unavoidable due to the presence of protein on or near the surface of fibers, resulting in an initial burst profile. Consequently, core-shell fibers are a preferred choice as they increase the distance between the protein and surface. An ideal system would consist of a core-shell arrangement in which there is diffusion across the shell and polymer degradation is set at a defined rate through the use of enzymes. To date, this ideal protein release has not been reported in the literature [47].

2.4 Material Selection

2.4.1 Poly(ε-Caprolactone)

PCL is a hydrophobic, semi-crystalline, aliphatic and biodegradable polyester approved by the US FDA as an implant material suitable for use in the human body. It is synthesized by a ring-opening polymerization of ε-caprolactone, which is derived from crude oil. This polymerization is illustrated in Figure 13.

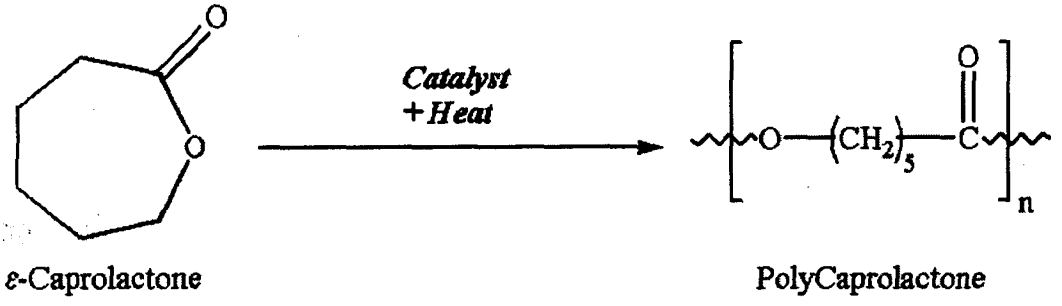

Figure 13 Chemical structure and ring opening polymerization of PCL

PCL is degraded by the hydrolysis of its ester linkages under physiological conditions. It has attracted increasing attention as a biomaterial for implanted medical devices and is particularly suitable for long-term devices due to its relatively slow degradation rate. PCL has been shown to be non-toxic to cells [71, 72]. Unlike commonly used biodegradable polymers such as PLGA, PCL does not produce a local acidic environment as it degrades. As such, the neutral degradation products of PCL provide a benign environment for pH sensitive proteins encapsulated in the polymer matrix. Furthermore, the inherent hydrophobic nature of PCL allows for a more effective controlled release of hydrophilic proteins, as PCL does not swell in the aqueous environments typical of cell culture.

PCL is most often used for electrospinning at a molecular weight of 80 kDa and concentrations in the range of 8-15% w/v. PCL scaffolds have been shown to maintain a high mechanical strength and structural integrity while excluding the need for chemical cross-linking using glutaraldehyde or other potentially cytotoxic chemicals. Specifically, the Young's Modulus and tensile strength of electrospun PCL have been shown to be 307 MPa and 58 MPa, respectively [73]. Lastly, compared to other synthetic biopolymers, such as PLA and PLGA, PCL has a much lower cost, making it more practical for various large-scale applications.

2.4.2 Trifluoroethanol

TFE, shown in Figure 14, is a water soluble organic solvent. The trifluoromethyl group on the compound is relatively electronegative, which aids in the electrospinning processes as it is repelled from the positive charge at the needle tip. It has a density of 1.393 g/ml and is able to dissolve peptides and proteins.

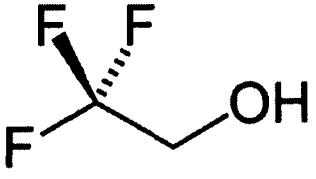

Figure 14. Chemical Structure of TFE

The boiling point of TFE is 78°C, therefore it is far less volatile than similar organic solvents used in polymer solutions, such as dichloromethane, which has a boiling point of

40°C. TFE has a successful history as an organic solvent for electrospinning and has been used to dissolve PCL [49, 74] as well as natural polymers [75].

2.4.3 Poly(ethylene glycol)

PEG is a well documented biocompatible polymer used in tissue scaffolds and displays excellent fiber forming properties [7, 44, 45, 49, 61, 76-78]. The stability of sensitive bioactive proteins is enhanced by the protective barrier provided by PEG and its presence may modulate the release characteristics of the protein. PEG has been used previously due to its ability to form pores in PCL to aid in the controlled release characteristics [44, 49, 78].

2.4.4 Bovine Serum Albumin

BSA was selected as a model protein to demonstrate the feasibility of incorporating bioactive macromolecules into PCL scaffolds. It was chosen based on its well-characterized size and biochemical stability. It has a mass of 66 kDa and is made up of 583 amino acid residues. It can be easily recognized by various sensitive protein assays and has a relatively low cost. Additionally, BSA is often used as a filler protein and stabilizer for many growth factors [44, 45, 49, 61].

The hydrodynamic diameter of BSA can be calculated using the Einstein-Stokes Equation, where η is the viscosity of the solvent, k is the Boltzmann constant, T is the

absolute temperature, and d and D_o are the hydrodynamic diameter and the diffusion coefficient of BSA, respectively: $D_o = kT / 3\pi\eta d$. The reported D_o value for BSA is 0.59 x 10-6 cm^2/s [79]. Using the Einstein-Stokes equation, the hydrodynamic diameter of BSA is 12 nm. This is important to consider when examining and evaluating the release of BSA through the PCL shell of coaxial nanofibers.

2.4.5 Platelet Derived Growth Factor

PDGF-BB is a protein that regulates cell growth and division. It contains two 109 amino acid residue chain monomers and has a molecular weight of approximately 25 kDa. The receptor for PDGF-BB is classified as a receptor tyrosine kinase, a type of cell-surface receptor. Upon activation by PDGF-BB, this receptor is turned on, which mediates the binding of various cofactors, activating specific signal transduction pathways. These pathways have downstream effects on the cell cycle, specifically, PDGF-BB can allow cells to bypass the G_1 checkpoint, causing cells to further divide rather than entering the G_0 quiescent state [80].

Previous *in vitro* work has shown that PDGF-BB stimulates proliferation of human fibroblasts and myofibroblasts. Pierce *et al* found that incision wounds treated with PDGF-BB generated a marked increase in GAG desposition, collagen formation and myofibroblast development [12]. Furthermore, the same study showed that PDGF-BB induced a quantitative increase in matrix synthesis compared to controls.

2.4.6 Transforming Growth Factor

TGF-β1 is a protein that plays a crucial role in tissue regeneration, cell differentiation, embryonic development and immune function. This cytokine was first identified in human platelets as a protein with two 112 amino acid residue polypeptides and a molecular weight of approximately 25 kDa, having a potential role in wound healing [10]. Not long after, TGF-β1 was characterized as a large protein precursor that gets enzymatically processed to form a functional protein [81]. TGF-β1 can inhibit the activity and secretion of other cytokines as well as decrease the expression levels of cytokine receptors to down-regulate the activity of certain cells. On the other hand, TGF-β1 can also increase the expression of certain cytokines and promote their proliferation, especially in cells that have not reached maturity [82].

Several studies have looked at specific repair mechanisms mediated by TGF-β1. Roberts *et al* found that injecting TGF-β1 into newborn mice induced angiogenesis [9]. They also found marked increases in collagen formation from fibroblast cell lines, which supports the role of TGF-β1 as an intrinsic mediator of collagen formation. It has also been shown that TGF-β1 preferentially triggers synthesis of collagen in early wounds and inhibits the differentiation of fibroblasts into myofibroblasts [12].

Finally, Ross *et al* recently showed that adult progenitor cells isolated from porcine and human bone marrow and treated with TGF-β1 alone or combined with PDGF-BB

induced differentiation towards smooth muscle cell phenotype and function [83]. This provides evidence that a scaffold capable of temporally and locally controlled release of these growth factors may be an ideal system to demonstrate the potential of cell recruitment and differentiation in tissue regeneration.

2.4.7 Radial Arterial Cells

RA cells are a type of vascular smooth muscle cell, which have shown promise as a cell source for cardiovascular tissue engineering efforts. This cell source has been shown to be both practical and highly viable, as research has shown that RA cells are able to actively remodel the ECM. These cells were previously shown to degrade an artificial collagen matrix and subsequently synthesize a natural collagen matrix, a process that is critical to effective tissue regeneration. RA cells have demonstrated positive staining for smooth muscle α-actin and smoothelin, consistent with the phenotypes of other vascular cell types, verifying the suitability of RA cells as a potential cell source for cardiovascular tissue engineering [84].

Chapter Three

3.0 Materials and Methods

3.1 Coaxial Electrospinning Apparatus

3.1.1 Design

In designing the coaxial electrospinning apparatus, a comprehensive literature review was performed in order to identify the types of equipment required as well as the most ideal characteristics sought for the specific application. Various arrangements have been reported in the literature. The most straightforward and user-friendly setup is the use of a dual syringe pump, in which the two solutions are combined into a common needle tip through the use of a micro-capillary. The dual syringe pump allows for independent flow rates of the core and shell polymer solutions, a process that has proven invaluable in the coaxial electrospinning process.

For all coaxial electrospinning performed in this study, the two polymer solutions were supplied to the concentric needle tip at independent flow rates using a dual syringe pump (Model 33, Harvard Apparatus). In order to create the concentric needle tip, two different needle diameters had to be selected. The syringe providing the shell material was connected to a 20-gauge stainless steel needle, which was cut to form a blunt end. The syringe providing the core material was connected to a flexible silica capillary tube with an inner diameter of 250μm. The silica capillary feeding the core material was inserted

through a small hole in the base of the syringe containing the shell material. The capillary tubing was then fed through the 20-gauge needle until it was flush with the metallic needle tip, forming a concentric ring inside the 20-gauge needle. Epoxy was used to hold the silica capillary in place.

The system described above was connected to the dual syringe pump as shown in Figure 15. The syringe pump was calibrated to the specific syringes used (1 mL, BD Scientific) based on the manufacturers protocol and was capable of providing two independent flow rates ranging from $7.3 \times 10^{-6} - 3.2 \times 10^{3}$ ml/hr. Finally, a high voltage power supply capable of providing the necessary electric field was connected to the system by fixing the negative end to the collecting plate and the positive end to the metallic 20 gauge needle tip.

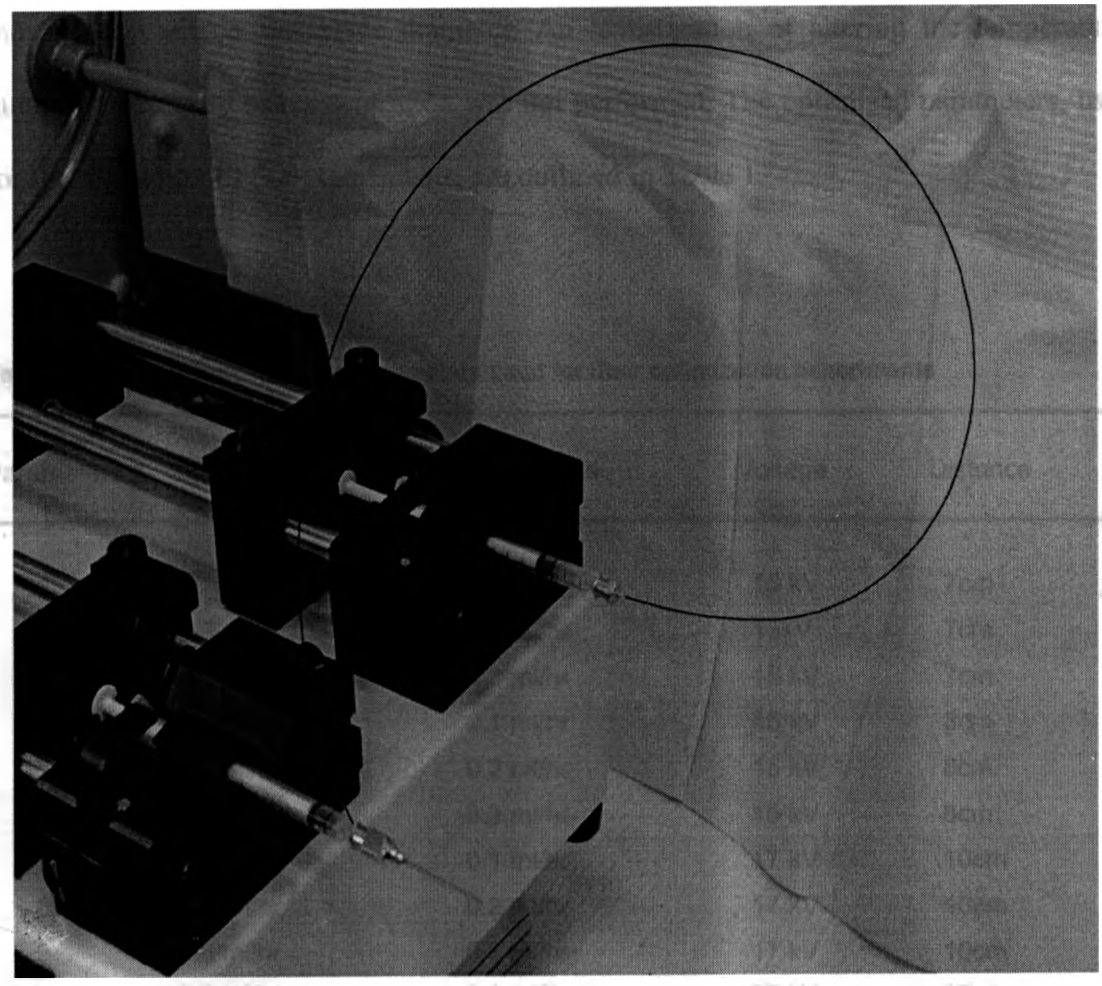

Figure 15. Digital photograph of the coaxial electrospinning setup in the lab

3.1.2 Parameters

A trial and error approach was used to determine the range of parameters within which continuous, uniform fibers could be formed at ambient temperature and humidity. In brief, the core and shell flow rates were experimented within a range of 0.1 to 0.6 ml/hr and 0.1 to 1.0 ml/hr, respectively. The selection of these rates is described in a later chapter. The electric field strength and the distance from the needle tip to collector were systematically altered in various experiments until fibers presented a uniform, bead free

morphology with a nanoscale diameter. An investigation of altering the temperature, humidity, viscosity or concentration was not performed. The optimized parameters, used for the remainder of the experiments, are outlined in Table 1.

Table 1 Coaxial electrospinning parameters used for fiber optimization experiments

Parameters	Shell Flow Rate	Core Flow Rate	Voltage	Distance
1	0.3 ml/hr	0.1 ml/hr	15 kV	7cm
2	0.3 ml/hr	0.2 ml/hr	15kV	7cm
3	0.3 ml/hr	0.3 ml/hr	15 kV	7cm
4	0.4 ml/hr	0.1 ml/hr	15 kV	8cm
5	0.4 ml/hr	0.2 ml/hr	15 kV	8cm
6	0.4 ml/hr	0.3 ml/hr	15 kV	8cm
7	0.6 ml/hr	0.1 ml/hr	17 kV	10cm
8	0.6 ml/hr	0.2 ml/hr	17 kV	10cm
9	0.6 ml/hr	0.3 ml/hr	17 kV	10cm
10	0.9 ml/hr	0.1 ml/hr	25 kV	10cm
11	0.9 ml/hr	0.2 ml/hr	25 kV	10cm
12	0.9 ml/hr	0.3 ml/hr	25 kV	10cm

3.2 Materials

3.2.1 Shell Polymer Solution

The shell solution was prepared by dissolving 6 grams of PCL (440744, Sigma-Aldrich) with a molecular weight of 80 kDa in 50 mL of trifluoroethanol (2,2,2-TFE Reagent Plus®, T63002, Sigma-Aldrich) in order to obtain a 12% w/v solution. Dissolution was achieved by mixing at room temperature for approximately 2 hrs.

3.2.2 Core Polymer Solution

3.2.2.1 Bovine Serum Albumin

The preliminary controlled release experiment involved using BSA (A9771, Sigma-Aldrich) that was conjugated with a fluorescent molecule, FITC, to aid in the fiber characterization. In brief, 5 grams of BSA-FITC was dissolved in 50 mL of double distilled water and mixed thoroughly to obtain a final concentration of 100 mg/mL. This concentration was chosen in order to optimize the processing parameters and fell within the range of concentrations used in the literature: 1 mg/mL [49], 10 mg/mL [45], 40 mg/mL [44] and 150 mg/mL [61].

The next controlled release experiment was carried out using a much lower concentration of non-fluorescent BSA (BP1605 Fraction V, Fisher Bio-Reagents®) in order to closer match the concentration of growth factor used in the final controlled release experiment. It was determined that growth factor loading at 1 μg/mL would be ideal for the cell culture experiments. Therefore, BSA was loaded at 10 mg/mL for modeling the controlled release, as this was the lower range of the detectable BSA concentration. This was among lowest concentrations used in the literature for controlled release from electrospun PCL fibers. In brief, 0.5 grams of BSA was dissolved in 50 mL of double distilled water and mixed thoroughly, to obtain a final concentration of 10 mg/mL.

3.2.2.2 Poly (ethylene-glycol)

PEG, with a molecular weight of 10 kDa, was added to the core solution in an effort to provide stability to the electrospinning process. In brief, 10 grams of PEG (309028, Sigma-Aldrich) was dissolved in the 50 mL BSA solution, described above, to obtain a final PEG concentration of 200 mg/mL.

3.2.2.3 Platelet Derived Growth Factor

Recombinant Rat PDGF-BB (520-BB, R&D Systems) was reconstituted to 50 μg/mL using 4mM HCl containing 0.1% BSA. This solution was left to fully dissolve overnight and was added to a 20% w/v PEG solution to a final concentration of 1 μg/mL. This solution was used as the core of the PDGF-BB coaxially electrospun scaffolds.

3.2.2.4 Transforming Growth Factor

Recombinant Human TGF-β1 (240-B, R&D Systems) was reconstituted to 25 μg/mL using 4mM HCl containing 0.1% BSA. This solution was left to fully dissolve overnight and was added to a 20% w/v PEG solution to a final concentration of 1 μg/mL. This solution was used as the core of the TGF-β1 coaxially electrospun scaffolds.

3.3 Scaffold Characterization

3.3.1 Scanning Electron Microscopy

The surface morphology, distribution and diameter of the electrospun coaxial fibers were characterized using SEM images. Images were acquired by a Leo 1530 SEM using an accelerating voltage of 2 kV, which was low enough to avoid damage to the samples while generating clear images with a high resolution.

3.3.2 Laser Scanning Confocal Microscopy

The structure of the coaxial BSA-FITC loaded nanofibers was examined using a laser scanning confocal imaging system (LSM-410, Carl Zeiss) equipped with an Argon/He/Ne laser and a Zeiss LSM 510 inverted microscope. All confocal fluorescence images were taken with either a 63x or 40x objective lens. Excitation and emission wavelengths for the FITC were 488nm and 633nm, respectively. Excitation and emission wavelengths for the Hoescht 33342 cell stain were 375nm and 461nm, respectively. Excitation and emission wavelengths for the Alexa Fluor 568 Phalloidin cell stain were 578nm and 600nm, respectively. All of the cell culture images were taken using a pinhole value of 22 and a capture time of 4 seconds where each frame was averaged 16 times. Contrast and brightness were varied using an automated optimization function.

3.3.3 In Vitro Protein Release

3.3.3.1 Fluorescence Spectroscopy

For the initial protein release study, coaxial PCL scaffolds containing BSA-FITC (n=9) were electrospun and weighed using the parameters discussed above. The scaffolds were immersed in 1mL PBS (pH = 7.4) at 4°C without shaking or stirring. At predetermined time intervals, the PBS release buffer was completely removed for analysis and 1mL of fresh PBS was added to each sample for the ongoing release measurements.

The BSA-FITC amount present in the release buffer was determined using a Fluorescence Micro-plate Reader (Version 4.51, Tecan Safire). The excitation and emission wavelengths were 485 and 535 nm, respectively. All measurements were performed in triplicate to ensure statistical suitability. In order to calibrate the sensitivity of the fluorometer, a calibration curve was generated to identify the detectable range of the BSA. Additionally, in order to quantify the BSA release, a standard curve was created using a BSA range of 0-50μg/mL, which is the range that the samples were expected to fall within. The standard curve, shown in Appendix A, was subsequently used to convert the fluorescence intensity to BSA mass.

3.3.3.2 Bradford Protein Assay

As a means to verify and further optimize protein loading and release from the coaxially electrospun scaffolds, a sensitive protein assay (Protein Assay Dye Reagent 500-0006,

Bio-Rad Laboratories Inc.) was used to measure the protein released from the scaffolds. The Bio-Rad protein assay, based on the method of Bradford [85], is an accurate procedure for determining the concentration of solubilized protein. It involves adding an acidic dye to a protein solution and subsequent absorbance measurement.

Scaffolds were immersed in 1mL of PBS and incubated at 37°C over a 168-hour period. The PBS was removed at various predetermined time-points and replaced with fresh PBS. The BSA concentration in the removed PBS supernatant was measured using the Bradford colorimetric method to determine the concentration of free BSA to assess the amount BSA released into the supernatant PBS solution. All measurements were performed in triplicate to ensure statistical suitability.

A BSA standard curve was prepared by measuring five BSA standard solutions (2, 4, 6, 8 and 10 μg/mL). All standard protein solutions were assayed in triplicate. For all samples, Bradford reagent was added to the PBS supernatant and the absorbance was measured at 595nm using a UV-Visible Light Spectrophotometer (DU-520, Beckman Coulter). Finally, a comparison of the absorbance level with the standard curve, shown in Appendix A, provided a relative measurement of protein concentration.

3.4 Cell Culture

3.4.1 Cell Isolation and Culture

RA cell isolation was performed as described earlier [84]. In brief, radial arteries were dissected out of porcine forelimbs in sterile lab conditions. The porcine radial arteries were minced into small pieces and digested in 0.08% collagenase (Sigma-Aldrich) for 24 hours at 37°C in a shaker bath. Culture tubes were then centrifuged for 5 min at 1100 rpm, and the resultant tissue pellet was re-suspended in Medium 199 (Invitrogen, Canada). Tissue pieces were plated onto 100-mm^2 dishes and cells were removed after substantial cellular outgrowth.

RA cells were cultured on 3 plates (each from a different animal: A, B and C) to maintain statistical variability (1 plate from 2^{nd} passage and 2 plates from 6^{th} passage). Each plate of cells was rinsed with 4mL of HBSS. Each plate received 2mL of 0.25% trypsin to loosen the cells. Cells were then assumed to be free-floating in the culture dishes and the solution from each plate was transferred to separate test tubes. Growth medium was added to each test tube, containing Dulbecco's Modified Eagle's Medium, Fetal Bovine Serum, and 1% Penicillin-Streptomycin. Test tubes were then centrifuged and the solution in each tube was replaced with 2mL of growth medium.

Each scaffold was sterilized under UV light for 1 hour and received 100uL from tube A, B or C. Therefore, cells were seeded at a density of 25,000 cells per scaffold. Scaffolds

were distributed into eighteen groups (six for each time period) to generate statistical variability. Tables 2 and 3 show the six groups distributed for each time period. The 24-well plates were placed in a humidified incubator at 37°C and 5% CO_2 for the duration of the experiment. After 24, 48 or 72 hours of incubation, cells on appropriate samples were fixed using 4% formaldehyde.

Table 2 Cell culture layout for RA cells seeded on scaffolds releasing PDGF-BB (triplicate study)

Control + A	Control + B	Control + C
PDGF + A	PDGF + B	PDGF + C
PDGF + A	PDGF + B	PDGF + C
PDGF + A	PDGF + B	PDGF + C

Table 3 Cell culture layout for RA cells seeded on scaffolds releasing TGF-β1(triplicate study)

Control + A	Control + B	Control + C
TGF + A	TGF + B	TGF + C
TGF + A	TGF + B	TGF + C
TGF + A	TGF + B	TGF + C

Cell staining was carried out by washing samples with a 1:100 dilution of Hoescht 33342 for the nuclei and with a 1:100 dilution of Phalloidin Alexa Flour 568 for the cytoskeleton. Samples were then cover-slipped using fluorescent mounting medium.

3.4.2 Cell Proliferation

In order to quantify proliferation of RA cells on each individual scaffold, confocal microscopy images were obtained in which the cell nuclei and cytoskeleton were stained. It was assumed that all cells on the sample had been adequately stained and each sample was imaged in five randomly selected locations. The number of cells in each image was quantified using Image Java software. The area of each image was 6400 μm^2 and a binary contrast algorithm provided by Image Java was used to differentiate between and count the cell nuclei.

Cell morphology and migration was evaluated by looking at confocal images from adjacent horizontal planes over a sample thickness of approximately 10μm. Images were also captured in which cells were migrating around individual fibers; as could be seen by the auto-fluorescence of PCL under certain confocal imaging parameters.

Chapter Four

4.0 Results and Discussion

The development of a novel tissue engineering scaffold capable of localized growth factor release relies on the optimization of both scaffold morphology and protein release kinetics. The initial challenge in this study was to fabricate uniform and continuous core-shell electrospun scaffolds through the process of coaxial electrospinning. Once the proper electrospinning parameters were acquired, the next challenge was to tailor the properties of the electrospun scaffold in order to achieve spatial and temporal control of protein release. This spatial and temporal control was identified and evaluated by the enhanced proliferation and migration of cultured RA cells on scaffolds releasing PDGF-BB or TGF-β1.

4.1 Optimizing Flow Rates

While optimizing the parameters used for coaxial electrospinning, it was found that controlling the flow rates of the core and shell solutions were particularly important, specifically the ratio between the two rates. In order to obtain a uniform, continuous, core-shell scaffold, optimum core and shell flow rates had to be determined experimentally. In the case of using a PCL shell and a PEG/BSA core, optimum flow rates were determined using a trial and error approach in order to obtain fibers with the smallest diameter while encapsulating the highest amount of BSA. This optimized

morphology was achieved using core and shell flow rates of 0.3 ml/hr and 0.6 ml/hr, respectively.

It was observed that a core flow rate below 0.1 ml/hr produced fibers with very low protein encapsulation, identified by extensive protein-void regions under confocal microscopy. Furthermore, using core flow rates above 0.3 ml/hr caused immediate electrospraying at the needle tip, as high amounts of hydrophilic PEG interfered with the hydrophobic PCL. This hydrodynamic instability caused the two polymers to electrospray onto the collector, forming no fibers.

The flow rate of the shell solution had an even more pronounced effect. When the shell flow rate was reduced below 0.3 ml/hr, the meniscus at the coaxial needle tip would not be fully formed and no fibers would be extruded from the tip. When the shell flow rate was increased above 0.9 ml/hr, the meniscus generated at the coaxial needle tip was too large for the electric field to overcome and no Taylor cone was formed, thus, the polymer solution would simply drip due to gravity and no fibers would be collected.

The above mentioned observations are outlined in Table 4, where 'S' represents electrospraying and 'D' represents dripping, in which the polymer solution simply dripped from the needle tip. The range within which uniform, protein-filled fibers were formed was found where the flow rates intersect at 'F'.

Table 4. Flow rate dependence chart showing the effect of varying the core and shell flow rate to obtain [S] Spraying [D] Dripping or [F] Fibers

Core Flow Rate (ml/hr) \ Shell Flow Rate (ml/hr)	0.1	0.2	0.3	0.4	0.6	0.9	1.0
0.1	S	S	F	F	F	F	D
0.2	S	S	F	F	F	F	D
0.3	S	S	F	F	F	F	D
0.4	S	S	S	D	D	D	D
0.6	S	S	S	D	D	D	D

Scaffolds that were created using a higher shell flow rate had an increased average fiber diameter as compared to those created using lower shell flow rates. This is likely due to the fact that decreased flow rates allowed the polymerous meniscus at the needle tip to be stretched into a sharper Taylor cone compared to that of increased shell flow rates.

This direct correlation between shell flow rate and fiber diameter is outlined in a subsequent section. In brief, using shell flow rates of 0.9, 0.6 and 0.4 ml/hr generated average fiber diameters of 492 ± 140, 336 ± 60 and 317 ± 114 nm, respectively. These results were consistent with those reported in the literature [49].

Core and shell flow rates in coaxial electrospinning have been shown to play a significant role in fiber morphology [43-45, 49, 61]. It was shown that using a core flow rate that was too low did not result in enough solution to supply the core of the fiber, resulting in a discontinuous core-shell structure. As the core flow rate was increased, the formation of a uniform core-shell structure was observed. On the other extreme, when the core solution flow rate was too high, the core solution at the concentric needle tip was no longer surrounded by the shell solution, causing spraying to spontaneously occur [86].

4.2 Scaffold Morphology

Once electrospun, the coaxial fibrous scaffolds were put onto glass slides for preliminary examination under an optical microscope. Typical scaffolds had an area of roughly $1cm^2$, as can be seen in Figure 16. This photograph shows an electrospun coaxial PCL-BSA fibrous scaffold, which was removed from the collecting plate and placed onto a glass slide for examination.

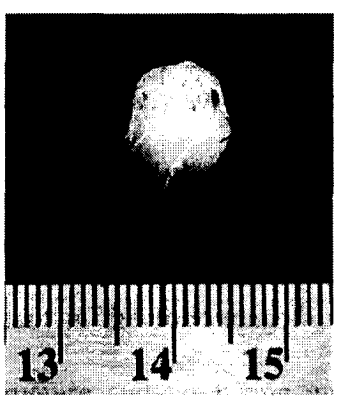

Figure 16. Digital photograph of coaxially electrospun PCL-BSA scaffold placed on glass slide immediately after electrospinning

Once observed under optical microscope, the morphological structure of the coaxially electrospun scaffolds was examined using SEM. As shown in Figures 17, 18 and 19, fibers showed a great deal of uniformity and continuity while maintaining a high level of porosity. Fiber diameter also showed a relatively distinct regularity in all samples. The fibers appeared to have a random orientation, as expected, and the topography appeared to be quite smooth. The scaffolds generated using the highest shell flow rate, Figure 17, appeared to have the roughest topography. This is likely due to the lack of stretching compared to the lower shell flow rates, shown in Figures 18 and 19. Using a higher shell flow rate did not allow the solution enough time to form a sharp Taylor cone, resulting in the observed rippled surface.

The scaffolds generated using the lowest shell flow rate, Figure 18, appeared to have a much smoother surface but there were some inconsistencies in the diameter of individual fibers, as can be seen in Figure 18-F. Finally, the fibers formed using a shell flow rate of 0.6 ml/hr, shown in Figure 19, had the most consistent diameter and a very smooth surface, while maintaining an ideal level of porosity.

In all samples, very few fibers contained any surface defects. Figure 17-B shows a minor defect, which was a rare morphological phenomenon, likely due to the aggressive processing conditions. There was significant interlacing and entanglement among the fibers in all samples, as is evident in the following figures. Nevertheless, all scaffolds displayed a true non-woven structure and no fusing was apparent between individual fibers at intersecting junctions or other overlapping regions.

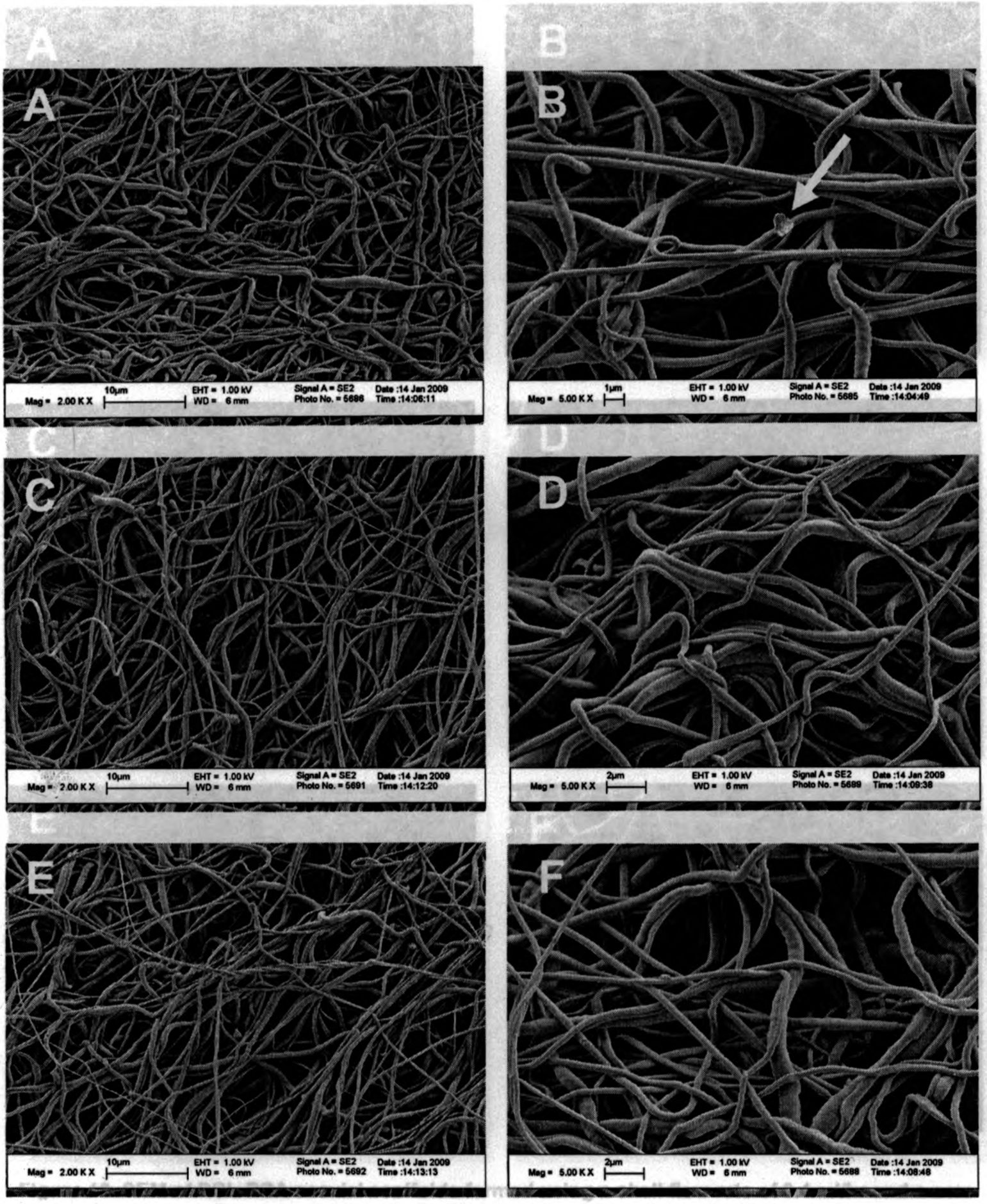

Figure 17. SEM of PCL-BSA coaxial scaffolds formed using a shell flow rate of 0.9 ml/hr and a core flow rate of 0.1 ml/hr [A,B], 0.2 ml/hr [C,D] or 0.3 ml/hr [E,F]

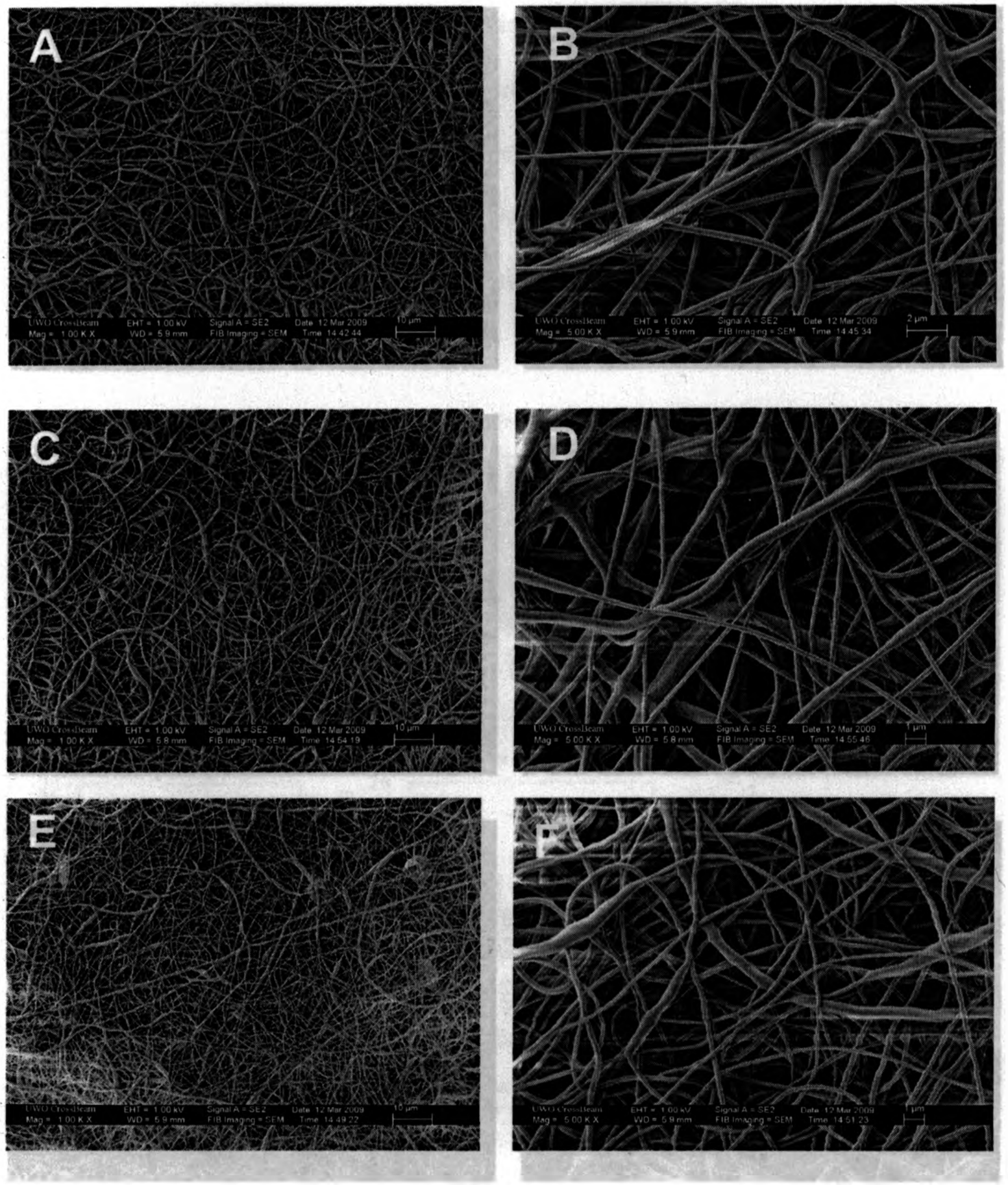

Figure 18. SEM of PCL-BSA coaxial scaffolds formed using a shell flow rate of 0.4 ml/hr and a core flow rate of 0.1 ml/hr [A,B], 0.2 ml/hr [C,D] or 0.3 ml/hr [E,F]

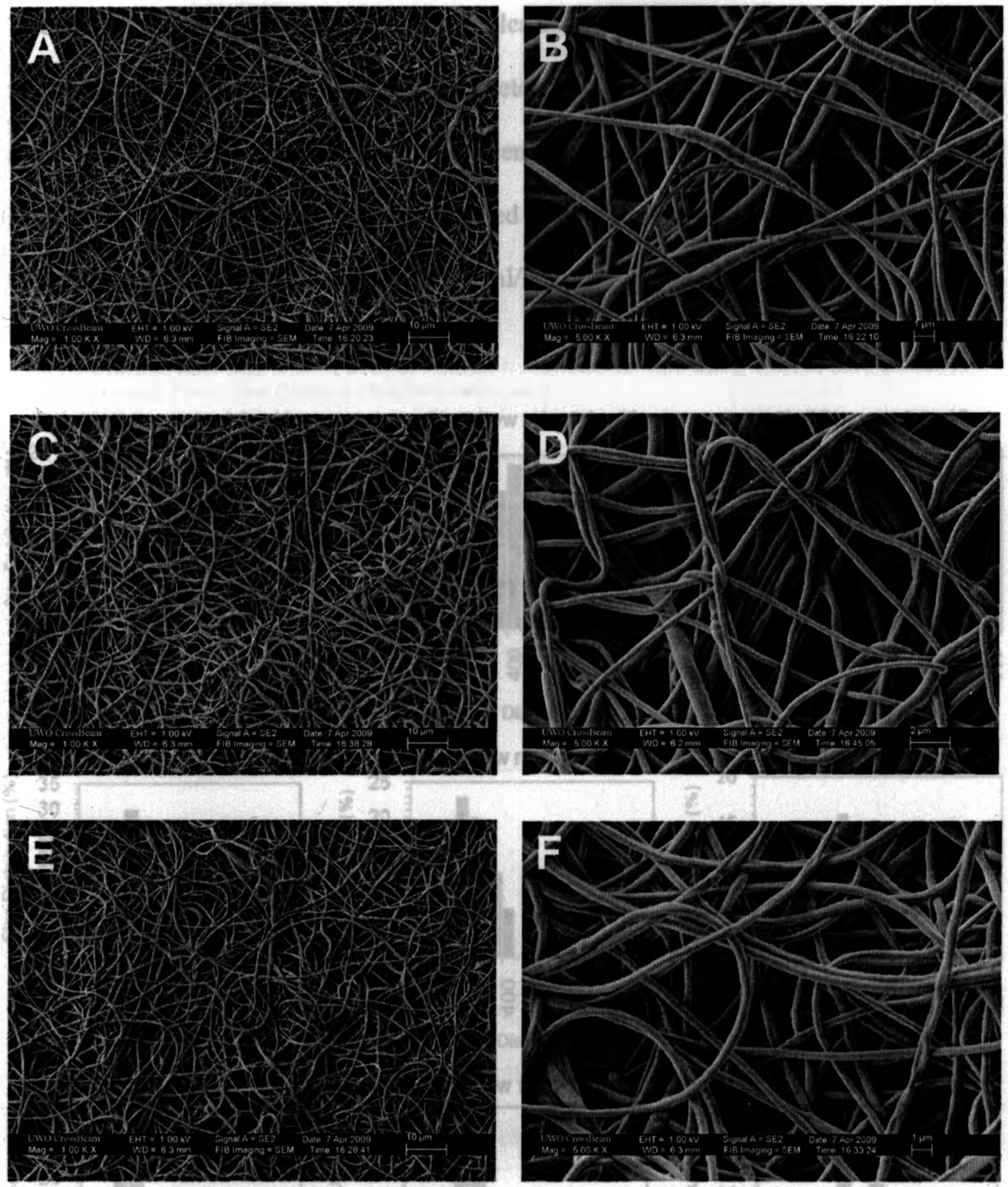

Figure 19. SEM of PCL-BSA coaxial scaffolds formed using a shell flow rate of 0.6 ml/hr and a core flow rate of 0.1 ml/hr [A,B], 0.2 ml/hr [C,D] or 0.3 ml/hr [E,F]

The diameter range of the fibers in all samples can be seen in the histograms below. The total range of fibers formed using all parameters ranged from 116 to 760nm. All samples appeared to have significant porosity between the fibers, although those generated using shell flow rates of 0.4 and 0.6 ml/hr appeared to have an increased porosity, compared to those formed using a shell flow rate of 0.9 ml/hr.

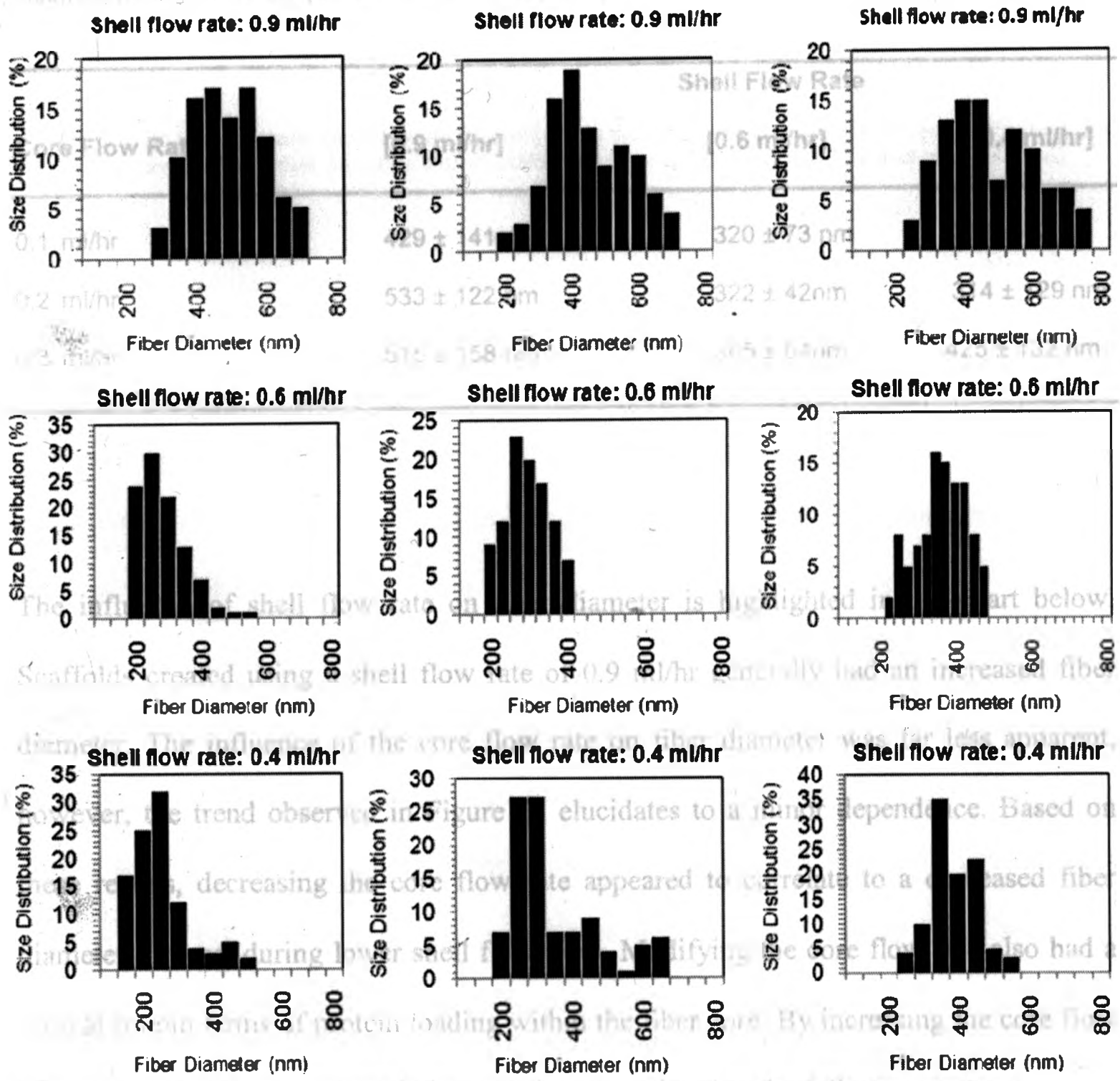

Figure 20. Histograms of fiber diameters for scaffolds formed using shell flow rates as shown and varying the core flow rates within each sample from 0.1 ml/hr [left column], 0.2 ml/hr [middle column] and 0.3 ml/hr [right column] corresponding to the SEM images above

The narrowest diameter range was achieved using a shell flow rate of 0.6 ml/hr and a core flow rate of 0.2 ml/hr, as shown in Figure 20-E. The widest diameter range occurred using a shell flow rate of 0.9 ml/hr and a core flow rate of 0.3 ml/hr, as shown in Figure 20-C. The average fiber diameters using the various parameters are outlined in Table 5.

Table 5 Average fiber diameter of coaxial PCL-BSA scaffolds formed using various core and shell electrospinning flow rates (Mean ± standard deviation)

	Shell Flow Rate		
Core Flow Rate	**[0.9 ml/hr]**	**[0.6 ml/hr]**	**[0.4 ml/hr]**
0.1 ml/hr	429 ± 141nm	320 ± 73 nm	212 ± 82 nm
0.2 ml/hr	533 ± 122 nm	322 ± 42nm	314 ± 129 nm
0.3 ml/hr	515 ± 158 nm	365 ± 64nm	425 ± 132 nm

The influence of shell flow rate on fiber diameter is highlighted in the chart below. Scaffolds created using a shell flow rate of 0.9 ml/hr generally had an increased fiber diameter. The influence of the core flow rate on fiber diameter was far less apparent, however, the trend observed in Figure 21 elucidates to a minor dependence. Based on these results, decreasing the core flow rate appeared to correlate to a decreased fiber diameter, at least during lower shell flow rates. Modifying the core flow rate also had a critical role in terms of protein loading within the fiber core. By increasing the core flow rate, protein loading consistently increased, as is outlined in the following section.

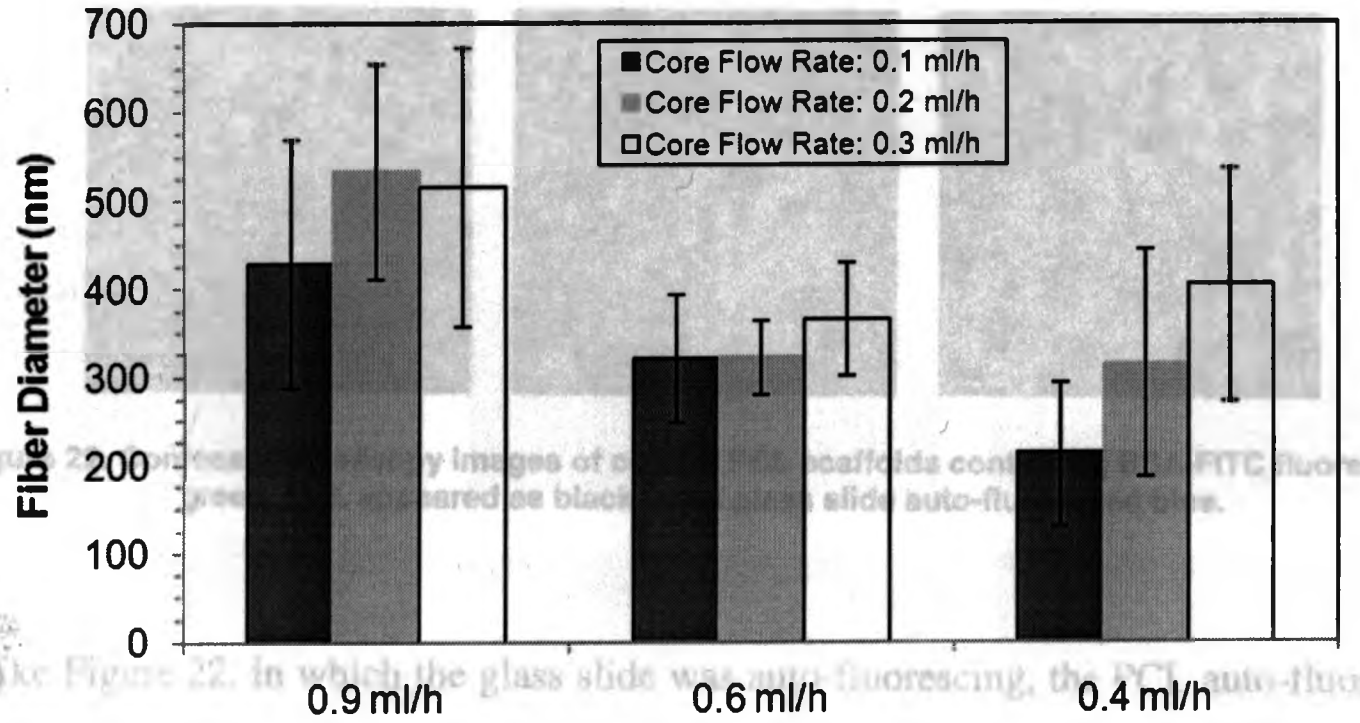

Figure 21. Fiber diameters for scaffolds formed using various core and shell flow rates, showing the dependence of various flow rate combinations of fiber diameter (Mean ± standard deviation)

4.3 Protein Loading

Since the SEM images are not capable of providing evidence that protein was successfully encapsulated into the core of the PCL fibers, protein loading was evaluated using confocal microscopy. The BSA encapsulated in the core was conjugated with a fluorescent molecule, FITC, which fluoresced green when observed under confocal microscopy using the parameters state above. The fibrous scaffolds were visualized in randomly selected locations under the confocal microscope using a 63x magnification objective lens. The green fluorescence from the BSA, apparent in Figure 22, became deeper with increasing amounts of the protein. All samples in Figure 22 were formed using a shell flow rate of 0.6 ml/hr and a core flow rate of 0.3 ml/hr. The following figures show continuous and uniform BSA within the fiber and were used to verify BSA loading.

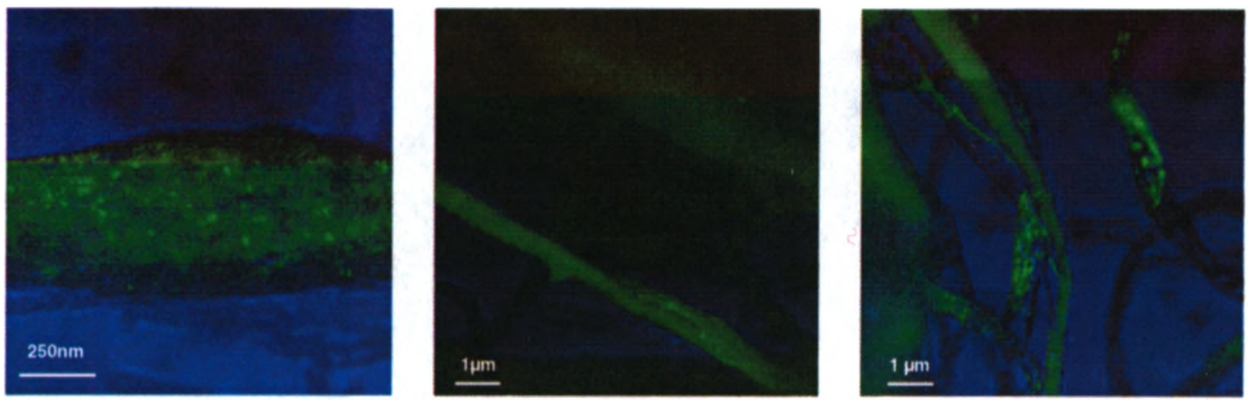

Figure 22. Confocal microscopy images of coaxial PCL scaffolds containing BSA-FITC fluorescing green. PCL appeared as black while glass slide auto-fluoresced blue.

Unlike Figure 22, in which the glass slide was auto-fluorescing, the PCL auto-fluoresced with a deep blue color under specific parameters, allowing for easy differentiation between the polymer and BSA. Figure 23 shows the scaffolds emitting both blue and green light, suggesting the presence of the labeled BSA within the PCL scaffolds. All images were taken of samples formed using a shell flow rate of 0.6 ml/hr. Different amounts of protein were observed depending on the flow rate of the core solution during coaxial electrospinning. This allowed for a qualitative interpretation of the protein continuity within the fibers, as well as the relative distribution of protein as identified by fluorescence intensity.

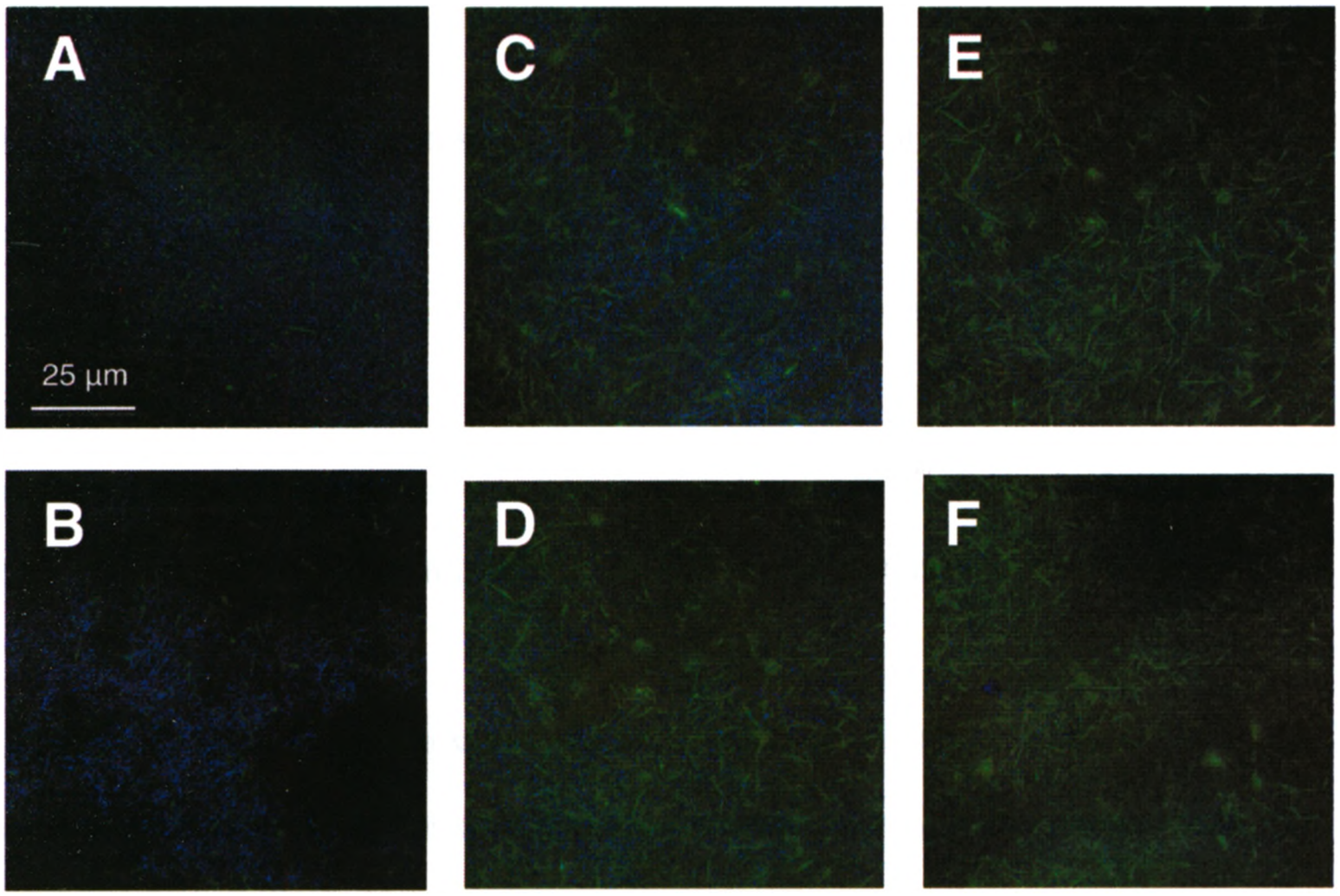

Figure 23. Confocal microscopy images of coaxial PCL-BSA-FITC scaffolds created using a shell flow rate of 0.6ml/hr and a core flow rate of 0.1 ml/hr [A,B], 0.2 ml/hr [C,D] or 0.3 ml/hr [E,F]

Figures 23-A and 23-B were taken of scaffolds formed using a core flow rate of 0.1 ml/hr. These figures show relatively few regions fluorescing green, suggesting that protein loading was non-continuous, leaving void regions in the fibers. Figures 23-C and 23-D were taken of scaffolds formed using a core flow rate of 0.2 ml/hr. The protein continuity appeared to be more stable in these samples although there were still numerous void regions. Images 23-E and 23-F were taken of scaffolds formed using a core flow rate of 0.3 ml/hr. The protein in these scaffolds had a suitable level of both uniformity and continuity, suggesting full encapsulation of BSA in the PCL fibers. This was also confirmed by the protein release experiments below.

4.3 Protein Release

The preliminary BSA release study was performed at 4°C using fluorescence spectroscopy over a 168-hour period. 4°C was chosen due to information supplied by the manufacturer regarding optimum BSA stability. The calculated BSA loading was 340 μg per scaffold, based on the core flow rate. In brief, coaxially electrospun scaffolds with an average mass of 1.5 ± 0.6 mg were immersed in 1mL of PBS, all of which was removed for analysis and replaced with 1mL of fresh PBS at predetermined time points (n = 9).

The PBS supernatant was analyzed using fluorescence spectroscopy, where the amount of BSA in the supernatant was recorded as fluorescence intensity. The intensity levels were converted to BSA amounts using a standard curve, shown in Appendix A, created using a series of solutions of known BSA-FITC concentrations. After the entire 7-day period, the total BSA released from each scaffold averaged 277 ± 42 μg which was roughly 81% of the total calculated protein loading. Figure 24 shows the cumulative protein release over the full period.

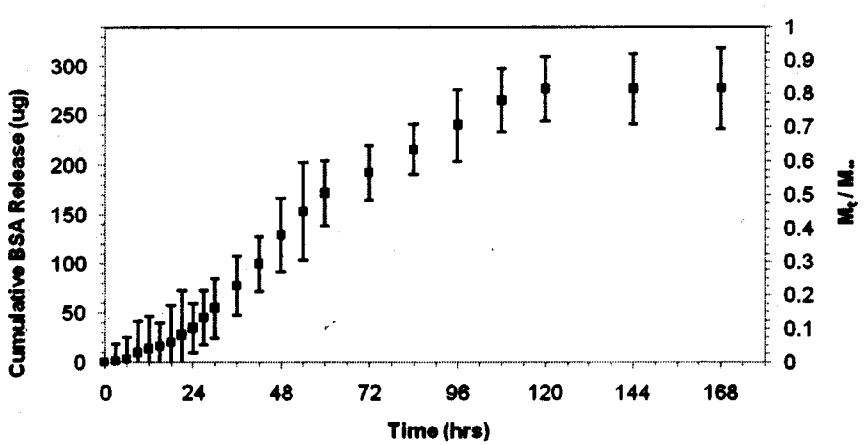

Figure 24. Cumulative release of BSA-FITC from coaxial PCL scaffolds in PBS at 4°C over 7-day period (Mean ± standard deviation). Calculated BSA-FITC loading was 340 μg while total BSA-FITC released was 277 ± 42 μg

4.3 Protein Release

The preliminary BSA release study was performed at 4°C using fluorescence spectroscopy over a 168-hour period. 4°C was chosen due to information supplied by the manufacturer regarding optimum BSA stability. The calculated BSA loading was 340 μg per scaffold, based on the core flow rate. In brief, coaxially electrospun scaffolds with an average mass of 1.5 ± 0.6 mg were immersed in 1mL of PBS, all of which was removed for analysis and replaced with 1mL of fresh PBS at predetermined time points (n = 9).

The PBS supernatant was analyzed using fluorescence spectroscopy, where the amount of BSA in the supernatant was recorded as fluorescence intensity. The intensity levels were converted to BSA amounts using a standard curve, shown in Appendix A, created using a series of solutions of known BSA-FITC concentrations. After the entire 7-day period, the total BSA released from each scaffold averaged 277 ± 42 μg which was roughly 81% of the total calculated protein loading. Figure 24 shows the cumulative protein release over the full period.

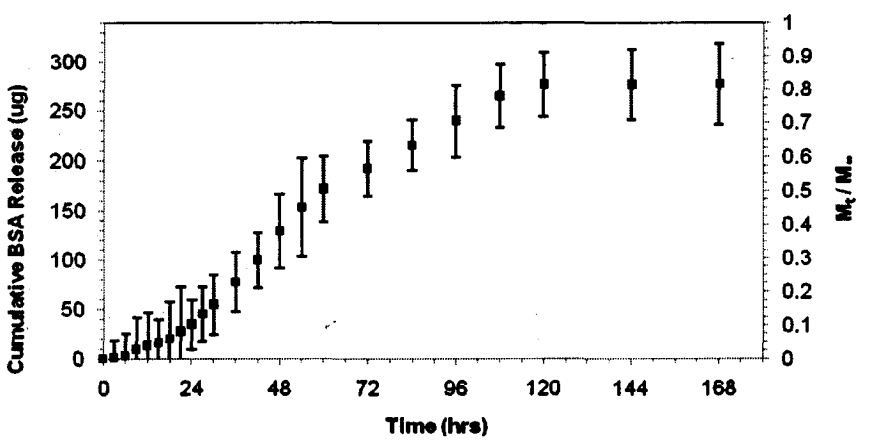

Figure 24. Cumulative release of BSA-FITC from coaxial PCL scaffolds in PBS at 4°C over 7-day period (Mean ± standard deviation). Calculated BSA-FITC loading was 340 μg while total BSA-FITC released was 277 ± 42 μg

The axis on the left side of Figure 24 shows the cumulative mass of BSA released from the scaffolds over the 168-hour period. The axis on the right side of the same figure shows the fractional release based on the calculated loading of 340μg of protein. As evident in this figure, the release essentially reached a plateau after 5 days, over which time, a diffusional release profile was observed. This release profile exhibited the classic characteristics of controlled release through a membrane [50].

Figure 25 shows the square-root time plot of the release profile, which was predominantly linear, reinforcing the diffusional characteristics of the system. As the BSA became depleted, after roughly 120 hours, the linear relationship was lost and a plateau was formed.

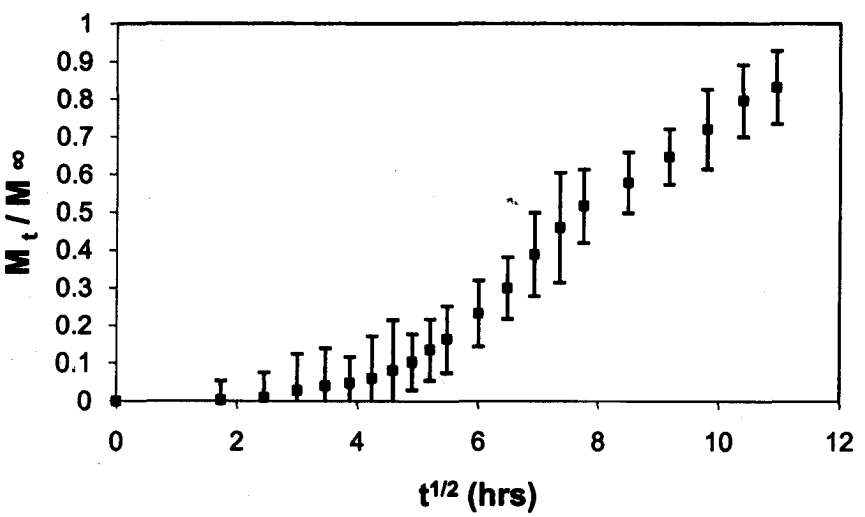

Figure 25. Square-root time plot of BSA-FITC release from coaxial PCL scaffolds. The linear region indicates diffusion-based protein release.

Due to the fact that tissue engineered constructs must be functionally suitable under physiological conditions, all subsequent protein release studies were carried out at 37°C and were evaluated using a more sensitive protein assay. Protein release in the coaxial PCL scaffolds was characterized by determining the amount of BSA released from the scaffolds over a 168-hour period. The calculated protein loading per scaffold was reduced to 50, 33 or 17 μg for samples made using core flow rates of 0.3, 0.2 or 0.1 ml/hr, respectively. Samples were created using shell flow rates of either 0.6 or 0.4 ml/hr. The reduction in core flow rate and protein loading was an effort to better mimic the low levels of protein used in the growth factor release experiments.

The BSA content in the PBS supernatant solution was evaluated by measuring absorbance using a UV-Visible Light Spectrophotometer based on the method of Bradford [85]. In brief, the BSA concentration was obtained using a standard curve, shown in Appendix A, created from a series of solutions of known concentrations. Data was compared to the standard curve to calculate the concentration and amount of BSA released.

Figures 26 and 27 show the BSA release profiles over a 72-hour period from the scaffolds created using a shell flow rate of 0.6 ml/hr. Data from the remainder of the time period was omitted because the release reached a plateau once the BSA was depleted or became entrapped in the PCL matrix.

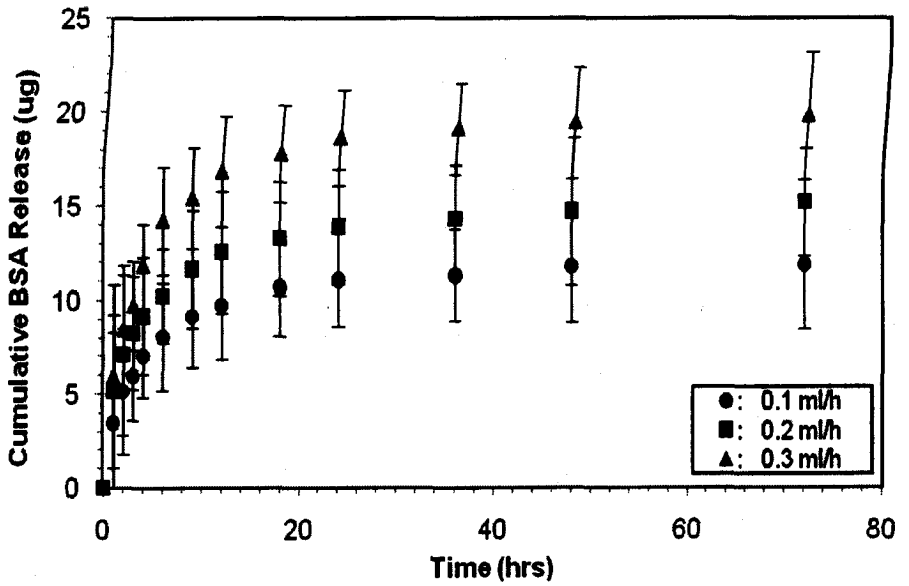

Figure 26. Amount of BSA released from coaxial PCL scaffolds formed using shell flow rate of 0.6ml/hr and various core flow rates shown (Mean ± standard deviation).

The release profiles for the first 72-hours, in all samples, were characterized as having a typical release pattern consisting of a burst release, followed by a sustained period of BSA release. Figure 26 shows the amount of BSA released from each of the samples. The amount of BSA released from samples prepared using core flow rates of 0.1, 0.2 and 0.3 ml/hr was 13 ± 3.4, 16 ± 2.9 and 21 ± 3.2 mg, respectively. Within the first 24 hours, the approximate percentage of the total protein released was 84, 86 and 88% for scaffolds created using core flow rates of 0.1, 0.2 and 0.3 ml/hr, respectively.

To assess the protein release kinetics, the fractional amount of protein released, based on calculated loading, was plotted against time. The fractional release, shown in Figure 27, was determined using the calculated loading levels. These levels were based on the amount of protein expected to be in the scaffolds under ideal conditions assuming that all of the protein was encapsulated.

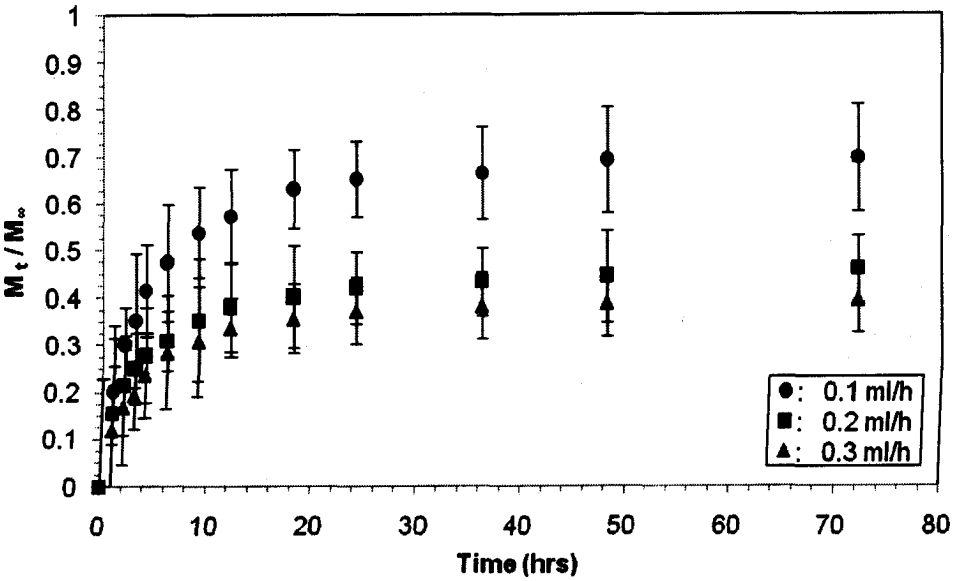

Figure 27. Fractional release of BSA from coaxial PCL fibers formed using a shell flow rate of 0.6ml/hr and various core flow rates shown (Mean ± standard deviation).

Based on the fractional release curve in Figure 27, the total release efficacy of these scaffolds was roughly 76, 49 and 42%, for scaffolds created using core flow rates of 0.1, 0.2 and 0.3 ml/hr, respectively. To further examine the release mechanics, the fractional release of protein was plotted against the square root of time, shown in Figure 28. This was generated using the above data, similar to the preliminary experiment, which assisted in characterizing the protein release.

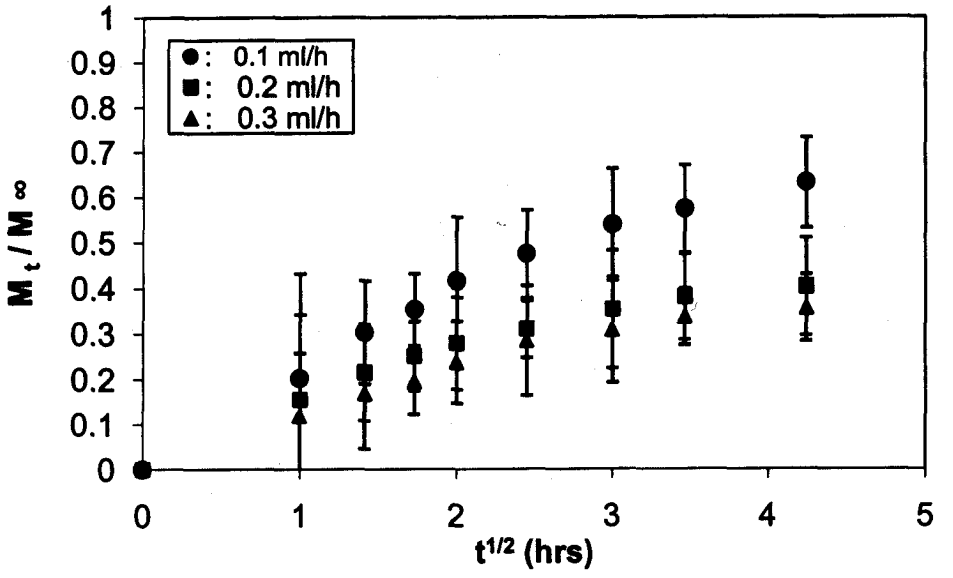

Figure 28. Square-root time plot of BSA release from coaxial PCL fibers formed using a shell flow rate of 0.6 ml/hr. The linear region indicates diffusion-based protein release.

According to the profile on the square-root time plot, shown in Figure 28, the primary mechanism responsible for the BSA release is, again, Fickian diffusion through the PCL shell. This is evident by the highly linear region of the square-root time plot over the first 18 hours of release, where the slope is proportional to the diffusion coefficient. Release subsequent to the first 18-hours was much slower and did not exhibit diffusional release. It was more indicative of protein entrapment within the PCL matrix, within nanopores in the scaffold.

In order to optimize the release characteristics, various samples underwent identical controlled release experiments using the same approach described above. The following results were obtained using all of the same parameters as above, although the shell flow rate was reduced from 0.6 ml/hr to 0.4 ml/hr and fewer time points were used.

Figures 29 and 30 show the BSA release profiles over a 72-hour period from the scaffolds created using a shell flow rate of 0.4 ml/hr. Again, data from the remainder of time period was omitted because the release reached a plateau once the BSA was depleted or became entrapped in the PCL matrix. The release profiles for the first 72-hours were characterized as having a similar typical biphasic pattern consisting of a burst release, followed by a sustained period of BSA release, similar to the previous result.

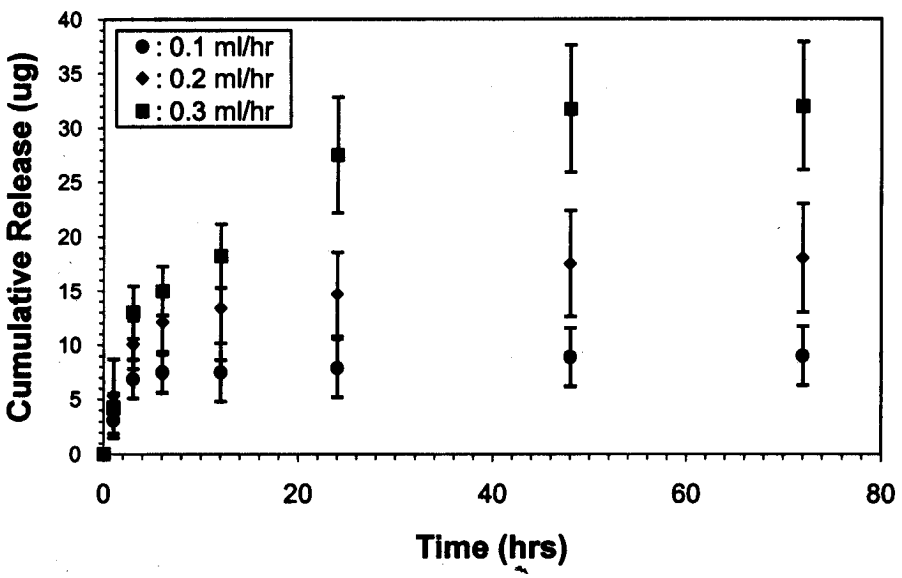

Figure 29. Amount of BSA released from coaxial PCL scaffolds formed using a shell flow rate of 0.4ml/hr and various core flow rates shown (Mean ± standard deviation).

The slopes obtained using these parameters were more gradual than those formed using the increased shell flow rate. Over the first 24 hours, the approximate percentage of the total protein released was 88, 82 and 86% for scaffolds created using core flow rates of 0.1, 0.2 and 0.3 ml/hr, respectively. Therefore, the burst release does not appear to have

worsened nor has it improved using these slightly different processing conditions. The following figure shows the fractional release of BSA from the scaffolds.

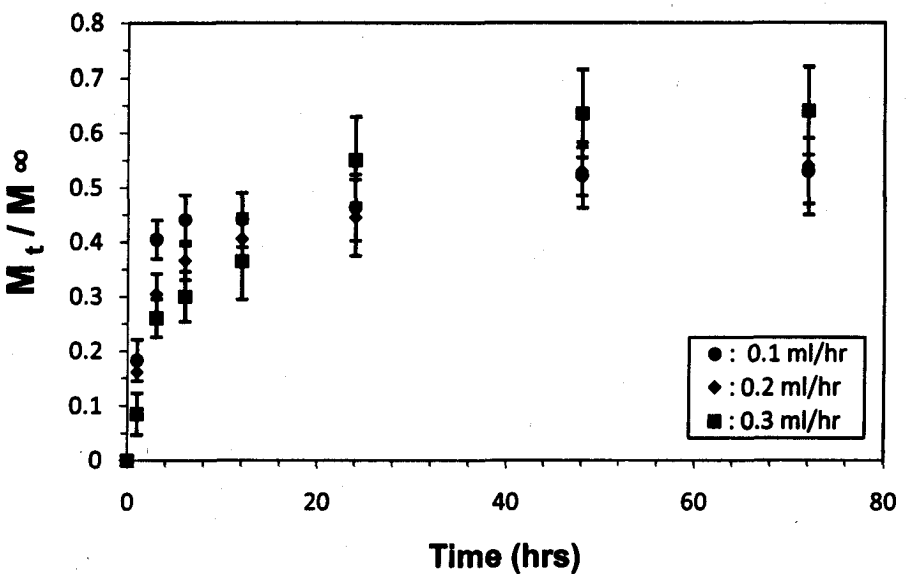

Figure 30. Fractional release of BSA from coaxial PCL scaffolds formed using a shell flow rate of 0.4ml/hr and various core flow rates shown (Mean ± standard deviation).

As with the results in the previous experiment, the fractional release profile provided a means to identifying the release kinetics and release efficacy. According to this profile, total release efficacy was roughly 53, 52 and 64%, for scaffolds created using core flow rates of 0.1, 0.2 and 0.3 ml/hr, respectively. Figure 31, below, shows a square root time plot of this data, which was used in evaluating the release kinetics. All samples appeared to have some degree of linearity on the plot although the samples created using increased core flow rates, 0.2 and 0.3 ml/hr, were more indicative of diffusional release, as their linearity is much more defined.

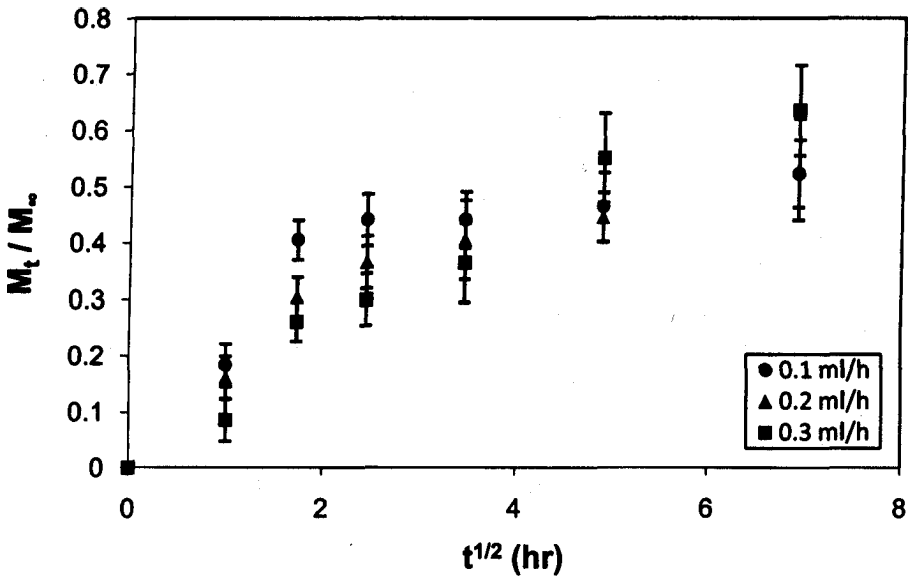

Figure 31. Square-root time plot of BSA release from coaxial PCL scaffolds formed using a shell flow rate of 0.4 ml/hr. The linear region indicates diffusion-based protein release. Scaffolds formed using a core flow rate of 0.3 ml/hr showed the most definitive diffusion-based release

The combined results from the two experiments described above are outlined in Table 6. The amount of protein released correlated well with the protein loading level, however, the protein release efficacy showed less correlation, suggesting that protein loading efficacy may not be ideal and that assumptions regarding the calculated loading levels may not have been accurate nor appropriate.

Due to the fact that these release efficacy levels are based on the calculated loading, it is important to note that they are not necessarily representative of the true efficacy of the scaffolds. True efficacy may be better evaluated by dissolving the scaffolds in a suitable solvent subsequent to the release experiment to measure the residual BSA in the scaffold.

Table 6. Protein release efficacy from coaxial PCL-BSA scaffolds formed using the various parameters shown. Calculated BSA loading was based on the assumptions stated above regarding ideal protein encapsulation.

Flow Rate [Shell]	[Core]	Calculated BSA Loading	Released Protein (Mean ± standard deviation)	Efficacy
0.6 ml/hr	0.1 ml/hr	17 μg	13 ± 3.4 μg	76%
0.6 ml/hr	0.2 ml/hr	33 μg	16 ± 2.9 μg	49%
0.6 ml/hr	0.3 ml/hr	50 μg	21 ± 3.2 μg	42%
0.4 ml/hr	0.1 ml/hr	17 μg	9 ± 2.7 μg	53%
0.4 ml/hr	0.2 ml/hr	33 μg	17 ± 4.8 μg	52%
0.4 ml/hr	0.3 ml/hr	50 μg	32 ± 5.8 μg	64%

Table 6 shows that the release efficacy of the scaffolds created using a higher shell flow rate increased with decreasing core flow rate. On the other hand, the release efficacy of the scaffolds created using a lower shell flow rate was shown to decrease with decreasing core flow rate.

Based on current understanding, this inconsistency cannot be explained by anything other than the possible discrepancy between calculated protein loading levels and actual total protein loading levels. Although fiber diameter was measured in all samples, the thickness of the shell encapsulating the protein was not measured. This thickness has important implications with respect to release kinetics because Fick's Laws of diffusion are dependent on the distance over which diffusion takes place. As such, obtaining quantitative measurements of the shell thickness could be a means to further characterizing the release profile.

Nevertheless, the results indicate that a significant amount of protein was released from the scaffolds with suitable temporal control subsequent to a slight burst release and the total amount released was directly proportional to calculated loading. This immediate release of protein from the scaffolds may be beneficial in certain circumstances in tissue-specific formation such as when cells require rapid, high concentrations of highly specific biological factors. Furthermore, eukaryotic cell migration is known to be mediated by chemotaxis, in which higher concentration gradients of chemotactic agents promote enhanced migration of eukaryotic cells.

The mechanism of protein release from a PCL matrix has not been clearly determined in the literature. It has been suggested that the moderately rapid release seen in many systems may be due to protein diffusion through the matrix wall [63]. This hypothesis is consistent with the present results and suggests that there may be ways of controlling the diffusional properties of the material through tailoring specific fiber forming parameters. It is thought that the remainder of the protein is likely trapped in the crystalline regions of the PCL and slowly releases as the polymer matrix degrades [87].

Another hypothesis put forward is desorption through nanopores in the polymer. In such a case, the limiting desorption stage would be accompanied by rapid diffusion as the supernatant solution filled in the nanopores. This theory was tested by Srikar *et al* and was found to be accurate in modeling the release from various polymers, including PCL, in which release efficacy ranged from 32 – 67% [67].

The controlled release of proteins such as growth factors from polymeric scaffolds is highly dependent on the geometry of the scaffold (fibrous, porous, etc), the properties of the polymer (molecular weight, cross-linking, hydrophobicity, etc), and the properties of the protein (solubility, size, surface charge, etc) [50]. The combination used in these studies employed bioactive proteins with an inert biodegradable polymer, which was engineered to regulate the duration and rate of release. This regulation was predominantly carried out through a diffusion-based controlled system, assuming no significant nanopores or surface defects existed on the surface. This type of delivery system is referred to as a matrix and reservoir, and is occasionally subject to several drawbacks.

Firstly, a premature release of protein from the device has been frequently noted in the literature. This study has attempted to alleviate this affect by introducing the protein to a hydrophobic polymer, known to slow the release of hydrophilic proteins. Secondly, these devices are often criticized as having a short therapeutic range. However, the purpose of the protein in this case was to provide a chemotactic environment to facilitate cell migration into the 3D scaffolds. Therefore, the localized range of growth factor delivery was well suited to the therapeutic requirements and purpose of this scaffold.

4.5 Cell Culture

4.5.1 Proliferation

The ultimate aim of this study was to evaluate the applicability of a scaffold that released growth factors, in the presence of cultured RA cells, as a tissue engineering construct. The RA cells seeded on the growth factor-loaded PCL scaffolds were compared to those seeded on inert PCL scaffolds after being cultured on the scaffolds for 24, 48 or 72 hours.

Cell proliferation was quantified by counting the number of cell nuclei within randomly selected 6400μm^2 regions of each scaffold. Figure 32 shows images of the RA cells cultured on PCL releasing PDGF-BB, PCL releasing TGF-β1, and control samples of pure inert PCL scaffolds after each of the three time periods. These images were taken using a confocal microscope under a 40x magnification objective lens. Each image represents an area of 6400 μm^2.

Figure 32 shows a dramatic increase in cell proliferation within scaffolds releasing PDGF-BB as well as those releasing TGF-β1, as compared to the control sample. It appeared as though the cells cultured in the presence of released growth factor reached a confluent state very quickly, whereas those cultured on the inert scaffolds were far less proliferative.

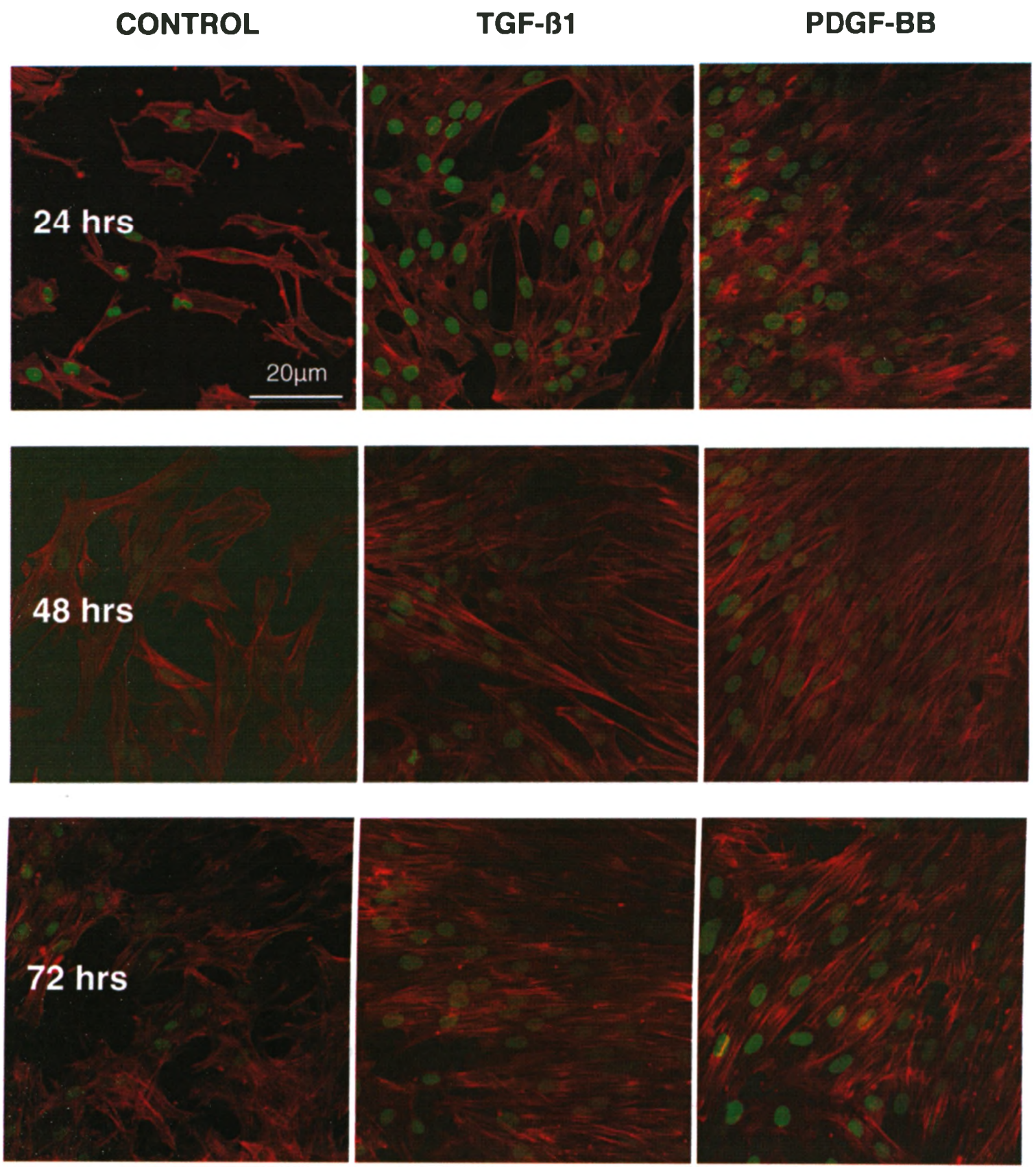

Figure 32. RA cell proliferation in the presence of TGF-β1 release or PDGF-BB release compared to inert PCL control after being cultured for 24, 48 or 72 hours.

The average number of cells, outlined in Table 7, within a 6400 μm^2 area of the control sample after the full 72 hours was 35 ± 3 whereas the average number of cells within the

same size area of the scaffolds releasing PDGF-BB and TGF-β1 were 55 ± 15 and 56 ± 19, respectively.

Table 7. RA cell proliferation after 24, 48 or 72 hours of culture on the various scaffolds (% compared to control)

Sample	24hrs	48 hrs	72 hrs
PCL + PDGF	254%	245%	157%
PCL + TGF	232%	218%	160%
Control (Pure PCL)	100%	100%	100%

If the control is taken to represent 100% proliferation, the RA cell proliferation was increased by roughly 154% in the presence of PDGF-BB release and roughly 132% in the presence of TGF-β1 release after 24 hours of culture. These results, plotted in Figure 33, suggested that cells were responding well to the localized growth factor release.

The data was analyzed using a one-way ANOVA, used to independently compare the means of each of the two groups with the control. Like many statistical tests, the results of this test can be considered reliable given that certain assumptions are met. The assumptions were that samples were random, variances among samples were equal, samples were independent and the data was normally distributed. The results of the one-way ANOVA indicated that proliferation of RA cells was significantly enhanced in the presence of controlled release of both TGF-β1 and PDGF-BB as compared to the control ($p < 0.05$, $n=3$).

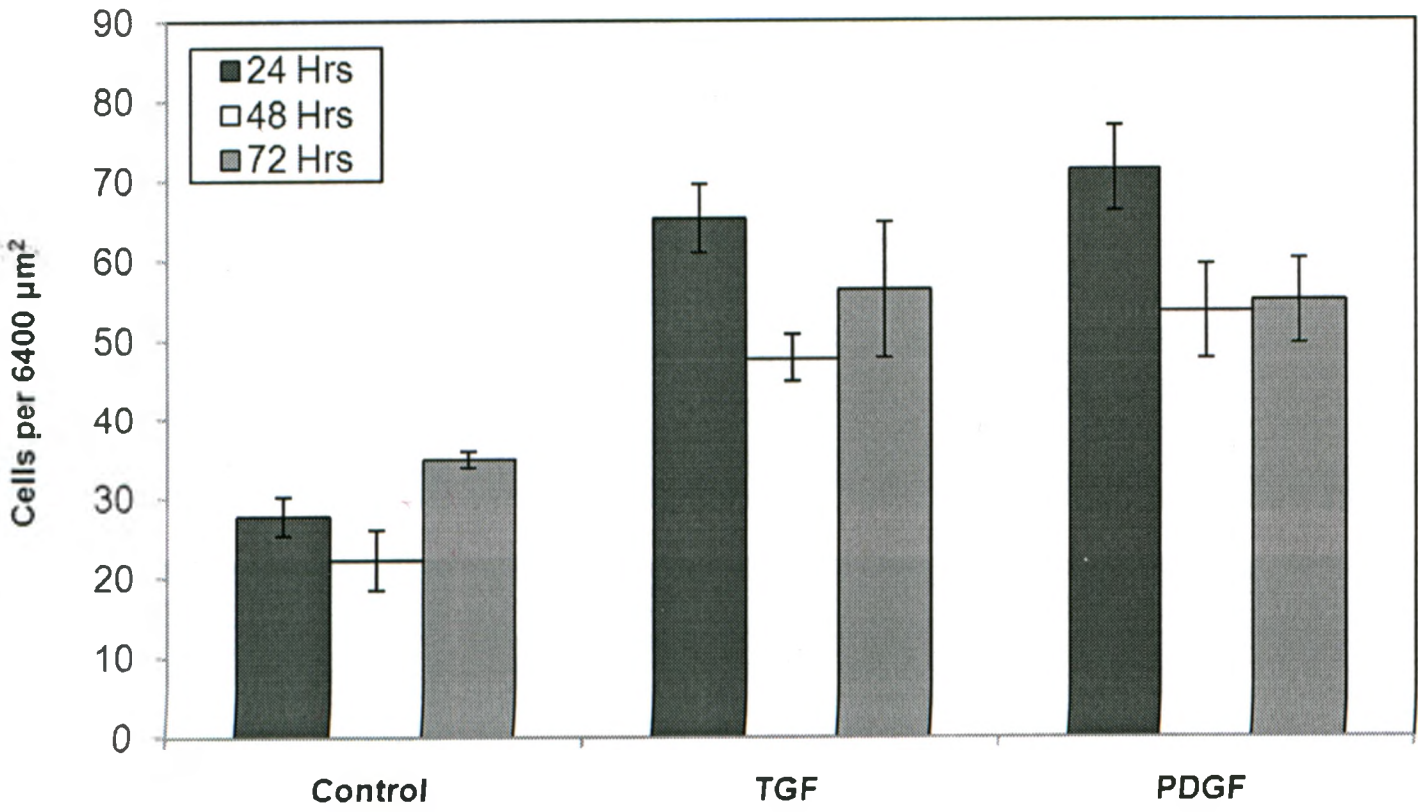

Figure 33. Cell nuclei count of RA cells cultured on PCL scaffolds releasing TGF-β1 or PDGF-BB compared to those cultured on inert PCL scaffolds after 24, 48 or 72 hours (Mean ± standard error)

4.5.2 Morphology and Migration

RA cells showed excellent cell attachment on all scaffolds, including the control. Cells were examined on the scaffold using confocal microscopy after 24, 48 and 72 hours of culture. The cells cultured on pure inert PCL showed a morphology suggesting satisfactory migration along the scaffolds, as shown in Figures 34-A and 34-B. The cytoskeletons showed significant stretching and focal adhesion points were apparent, as is clearly evident in Figure 34-B.

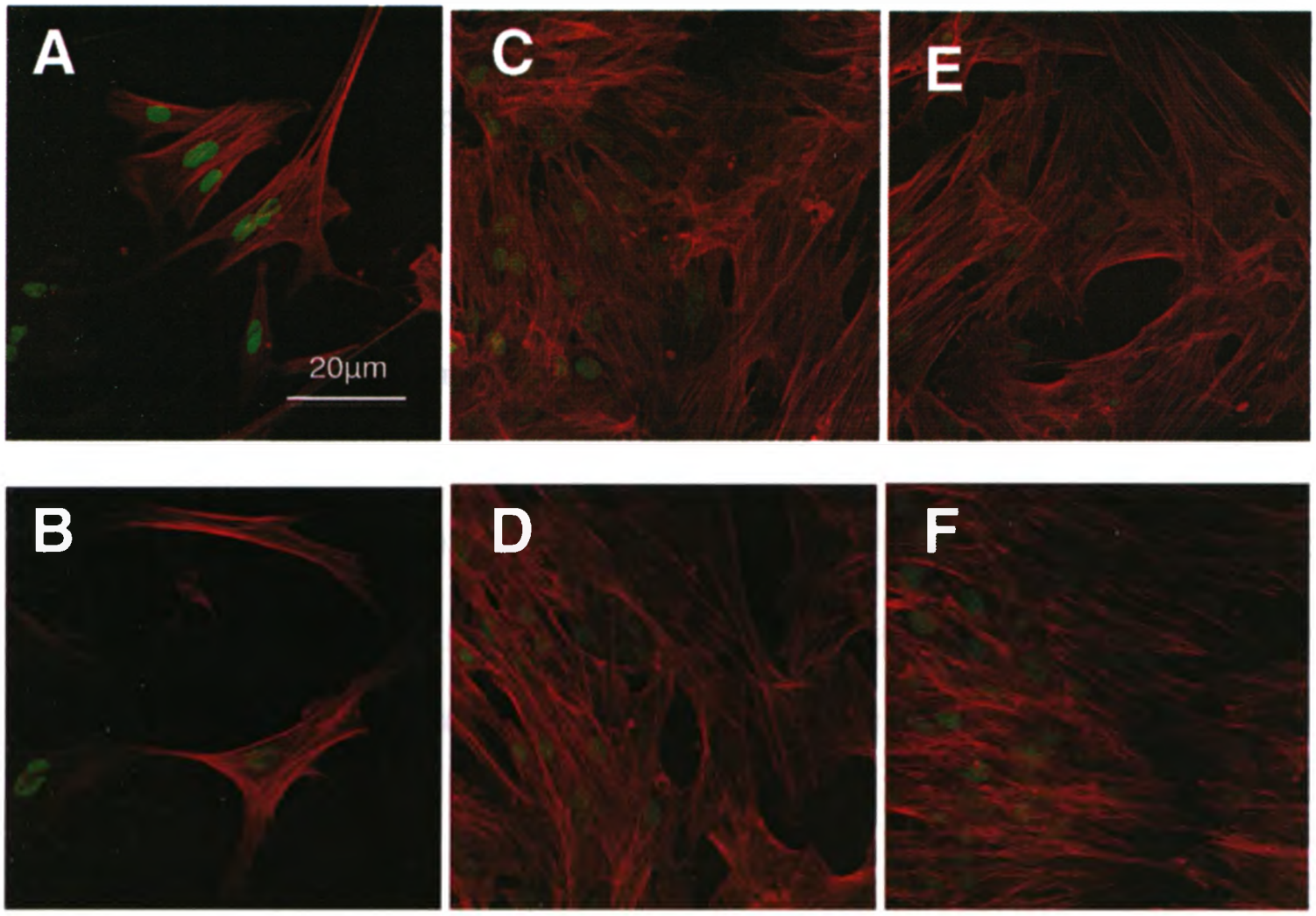

Figure 34. Confocal microscopy images of RA cells cultured on inert PCL scaffolds [A,B] compared to those cultured on coaxial PCL scaffolds releasing TGF-β1 [C,D] or PDGF-BB [E,F] after 48 hours

The cells cultured on the composite scaffolds releasing growth factor showed a morphology suggesting high levels of both migration and proliferation, as shown in Figure 34 (C-F). Cell density was extremely high and cells appeared to be extending and adhering well to the scaffold. The cells also appeared to be orienting themselves in a preferential direction based on a visual inspection, as can be seen in Figure 34-F. Although the shape of the cells varied considerably, most cells exhibited some level of motility and portrayed the characteristic bipolar morphology associated with migration. This morphology is due to the extension of cellular actin filaments through rapid actin polymerization. These filaments are the active force in cell motility and are often used to identify migrating cells. Due to the high density of bipolar cell morphology seen in the

cells exposed to TGF-β1 and PDGF-BB, compared to the control, it was apparent that cells were migrating in response to the preferred culture conditions incorporating the released growth factor.

Many of the cells cultured on scaffolds releasing TGF-β1 or PDGF-BB not only showed high levels of migration and appeared to migrate towards one another, but also appeared to migrate within the scaffold. Figure 35 shows cells within the individual pores of the fibrous scaffolds, suggesting a moderate level of interaction between the cells and scaffold, as well as a moderate level of infiltration into the 3D pores of the nanostructure.

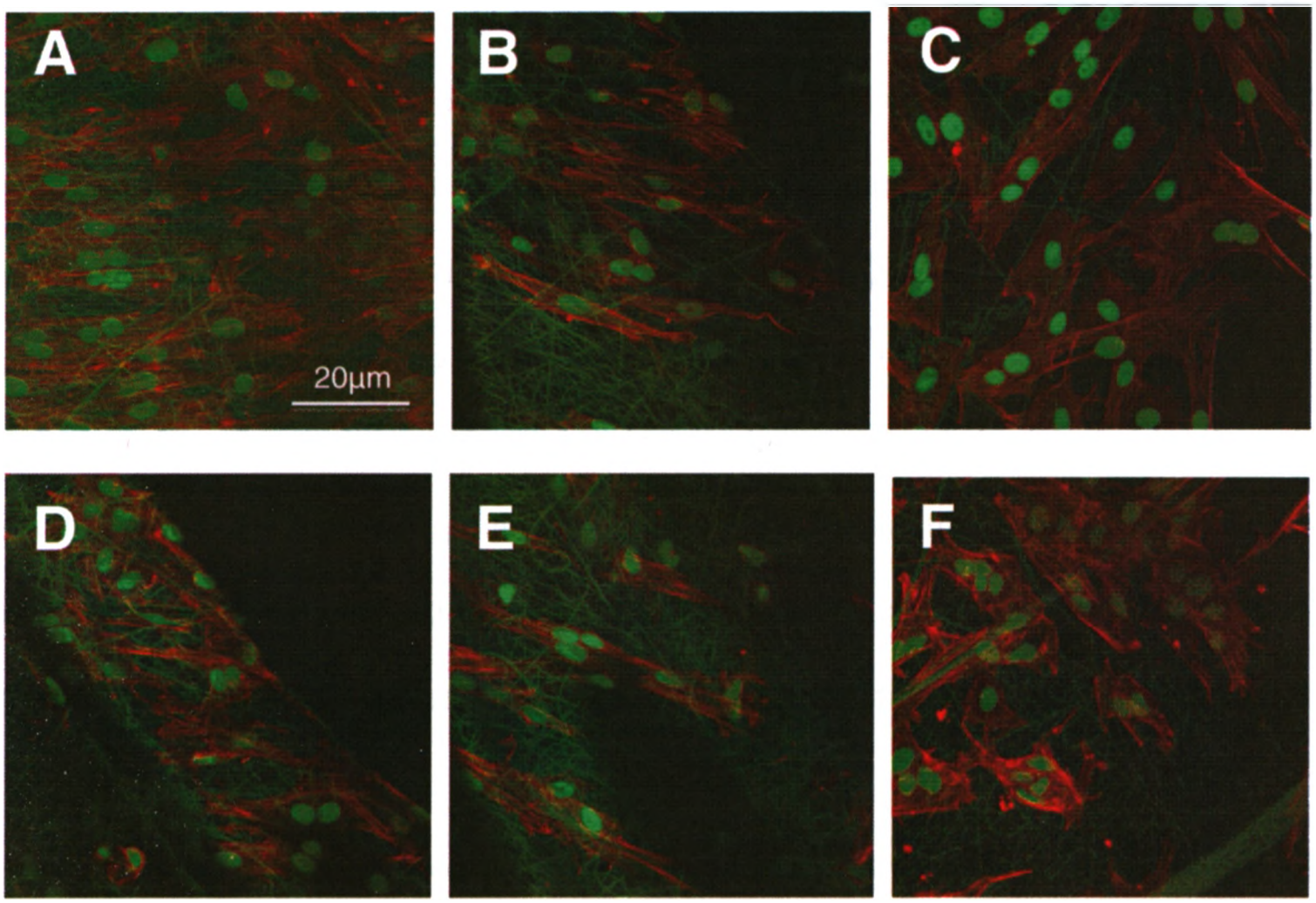

Figure 35. Confocal microscopy images of RA cells migrating within the 3D fibers of scaffolds releasing TGF-β1 [A-C] and PDGF-BB [D-F] after 48 hours of cell culture

Although the chemical response within the cells that drives them to migrate is still unclear, it has been hypothesized that the chemotactic gradient generated by the growth factors is sensed by the cells. This likely results in an intracellular gradient, initiating a signaling pathway, responsible for promoting the polymerization of actin filaments necessary for cell motility. The natural ECM provides a chemotactic reservoir *in vivo*, as chemo-attractant ligands are bound to the matrix, inducing natural migration of all sorts of cell types. The cell morphology observed in this study undoubtedly justifies these interactions as the development of growth factor concentration gradients resulted in significant RA cell recruitment.

Due to the fact that the specific growth factors used in these studies are known to promote a chemotactic effect, it was expected that a certain degree of cell migration and infiltration would be observed. Both PDGF-BB and TGF-β1 provided this chemotaxis by generating chemical gradients within the scaffolds, which likely guided the movement of cells based on the gradients. These chemical gradients were likely detected by the cells, resulting in a dynamic and polarized distribution of actin filaments, causing them to migrate preferentially toward the chemotactic PDGF-BB or TGF-β1. As can be seen in the following confocal images, cells were not only found migrating into the depths of the 3D scaffold, but were also observed wrapping around individual fibers. Since these scaffolds were releasing potent chemotactic agents, it was not surprising to see this intimate cell-scaffold connection and it was a very encouraging observation.

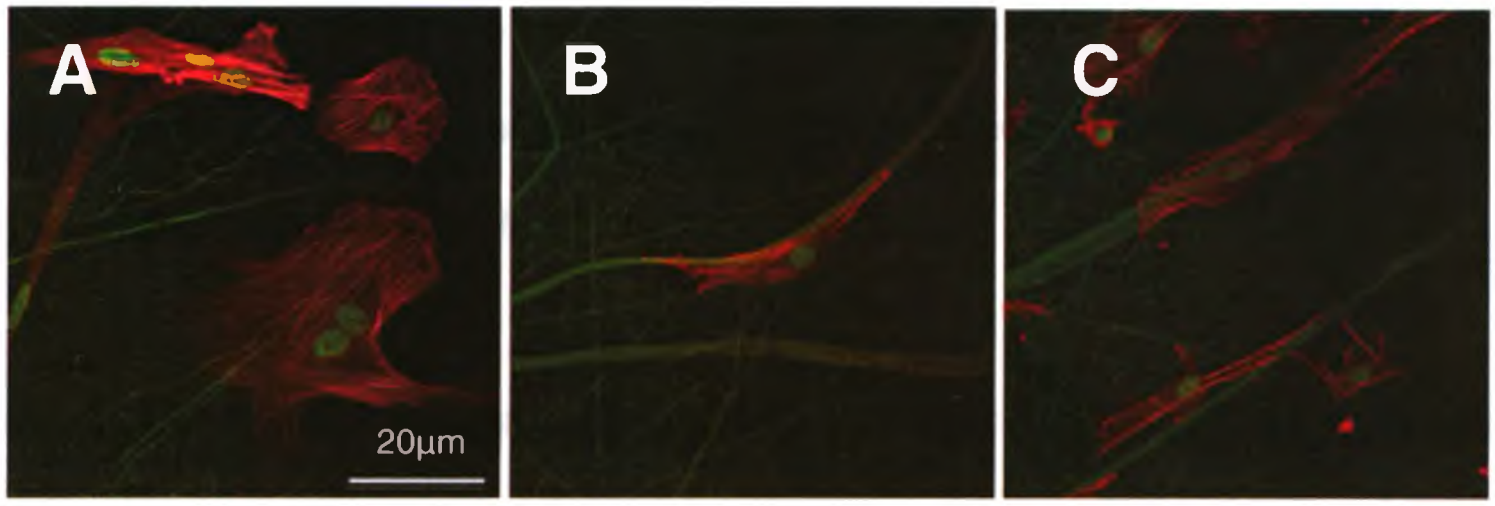

Figure 36. Confocal microscopy images of RA cells adhering to individual fibers of coaxial PCL scaffolds releasing PDGF-BB after 48 hours of cell culture

Various regions of both composite scaffolds showed proliferation to the point of confluence, however, this was not observed in any regions of the control scaffold. Figure 37 shows regions where cells formed large confluent pockets, which occurred throughout all of the composite scaffolds.

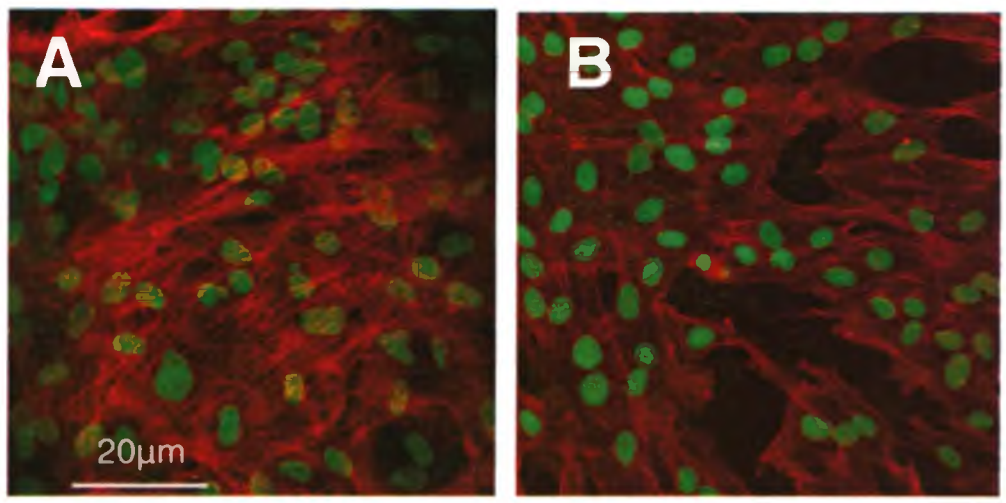

Figure 37. Confocal microscopy images of RA cells reaching confluency on scaffolds releasing TGF-β1 [A] and PDGF-BB [B] after 72 hours of culture

These highly confluent regions may be a result of cells migrating along concentration gradients of growth factor deposition or could indicate that cells underwent a highly

proliferative state in the presence of released growth factor. The level of confluency in many of these images suggested that there was little or no restriction to the proliferation of the cells, indicative of preferential culture conditions.

Overall, the experimental results suggested that, although the cells adhered and migrated on inert PCL scaffolds, exposure to the controlled release of PDGF-BB and TGF-β1 significantly enhanced the proliferation as well as migration within the fibrous constructs.

The coaxial PCL scaffolds releasing growth factor at a controlled rate appropriately mimic natural chemotaxis and thus provide a suitable environment in which to facilitate cell migration within the 3D scaffolds. One of the primary challenges in tissue engineering is inducing cell migration throughout the depths of 3D scaffolds to support tissue formation and function. The scaffold system reported here can potentially solve the problems associated with poor cell invasion and penetration. Not only does this scaffold have excellent biocompatible properties, but it also contains well-interconnected pores capable of facilitating cell migration throughout its network of growth factor-releasing fibers. This design offers a beneficial substrate for cell migration and matrix deposition, while facilitating mass transfer of nutrients and waste between the scaffold, the cells and the surrounding environment. Furthermore, unlike chemically conjugating bioactive molecules to the surface, the incorporation of growth factor within the scaffold has allowed them to retain their bioactivity, while not interfering with the microstructure of the scaffold.

Chapter Five

5.0 Conclusions and Future Work.

Despite years of research in the field of tissue engineering, results to date have been largely empirical. Among the reasons for suboptimal outcomes in generating functional tissue is the inadequate protein delivery at a micro-scale level during cell culture. The studies performed within this thesis aimed to bridge the gap between the use of bioactive molecules and scaffolds to better integrate them in tissue engineering efforts.

During the natural process of tissue repair, a very complex and well orchestrated release of cytokines is delivered to cells to promote proliferation, macrophage activation, angiogenesis and other important functions. The temporal control of these proteins is mediated by formation or repair processes, which occur naturally in every tissue within the body. One challenge in tissue engineering is to mimic these repair processes.

There are several crucial elements to consider when designing a system of high spatial and temporal complexity, in which biologically sensitive molecules are being used. Besides the morphology of the scaffolds, protein loading capacity and distribution as well as protein release kinetics and stability are crucial and were studied in order to evaluate the constructs as suitable tissue engineering scaffolds.

This study identified coaxial electrospinning as a suitable means for incorporating potent growth factors into cytocompatible PCL scaffolds, to better mimic the physiological architecture and processes throughout natural tissue repair. This novel technology appears to satisfy the void that currently exists in the tissue engineering process, that is, the lack of a suitable protein delivery mechanism. The ability to incorporate potent growth factors during scaffold fabrication offers extensive benefits for controlled delivery during tissue-specific formation.

This study showed that scaffold morphology exhibited the desired non-woven, bead free, fibrous structure. It was quickly determined that the shell flow rate during coaxial electrospinning was highly influential on the overall fiber diameter, while the core flow rate influenced protein continuity and uniformity. Next, protein release studies verified the controlled release of a model protein, BSA, in release buffer solutions. These studies suggested that protein loading efficacy above 50% is achievable under specific scaffold processing conditions. Furthermore, BSA release from PCL scaffolds at 37°C was sustained over a 72-hour period and exhibited a diffusion-based release profile.

Cells cultured on scaffolds containing PDGF-BB or TGF-β1 showed a significant increase in proliferation compared to the inert PCL control. Additionally, cell migration was enhanced by the use of these bioactive molecules, as cells were shown to wrap around fibers and penetrate within the bioactive PCL scaffold. Lastly, the proliferation

and migration results suggested that protein bioactivity was retained throughout the electrospinning process.

Due to improvements in processing technologies, the past five years have seen tremendous progress within the area of protein delivery for tissue regeneration. Due to the efforts by many research groups, coaxial electrospinning has emerged as a technique capable of processing a rich variety of materials into nanoscale composite fibers for many useful applications. With the progression of novel tissue engineering scaffolds, the future will lend itself to developing improved protein delivery systems, capable of providing more versatile release systems for guiding cell proliferation and migration.

This study has provided new insight into the fundamental cell-scaffold relationships resulting from controlled protein delivery using nanofibers derived from coaxial electrospinning. Going forward, scaffolds used for tissue engineering are expected to benefit dramatically from a shift towards the use of bioactive scaffolds providing a dynamic environment of growth factor delivery. Making use of the versatility of a growth factor delivery system is sure to revolutionize current capabilities and provide an improved platform for ongoing tissue regeneration efforts.

At the current stage of development, numerous technical issues still need to be resolved. However, there is no doubt that this technology is a process of choice for the development of functionalized bioactive scaffolds. Before this vision can be realized, it is

still necessary to systematically investigate the correlation between the secondary structure of core-shell electrospun scaffolds and the specific processing parameters by which they are fabricated. In order to fully achieve their full potential as growth factor reservoirs, it is crucial to systematically isolate parameters and understand how each parameter governs the morphological transformation in terms of core-shell uniformity and continuity.

This study has laid the groundwork for a novel tissue engineering scaffold capable of delivering bioactive growth factors *in vitro*. Future work must be directed in the systematic investigation of cellular interactions with the bioactive scaffolds and their response to localized growth factor release at the genetic level. Performing a detailed analysis of mRNA through the use of a reverse transcription polymerase chain reaction (RT-PCR) could be useful in identifying ECM protein deposition and other desirable properties of the bioactive constructs.

Finally, as tissue formation is driven by the cooperative stimulation of multiple growth factors working in concert to orchestrate a culmination of cellular events, the use of multiple growth factors in a single system should be investigated. This would further mimic the role of the ECM *in vivo* and would provide a site not only for cellular proliferation and migration, but would potentially aid in selective cellular differentiation efforts.

Chapter Six

6.0 References

1. Lutolf, M.P. and J.A. Hubbell, *Synthetic biomaterials as instructive extracellular microenvironments for morphogenesis in tissue engineering.* Nat. Biotechnol, 2005. **23**(1): p. 47-55.

2. Quaglia, F., *Bioinspired tissue engineering: the great promise of protein delivery technologies.* Int J Pharm, 2008. **364**(2): p. 281-97.

3. Babensee, J.E., McIntire, L.V. and Mikos, A.G., *Growth factor delivery for tissue engineering.* Pharm Res, 2000. **17**(5): p. 497-504.

4. Whitaker, M.J., Quirk, R.A, Howdle, S.M. et al., *Growth factor release from tissue engineering scaffolds.* J Pharm Pharmacol, 2001. **53**(11): p. 1427-37.

5. Li, C., Vepari, C., Jin, H. J., Kim, H. J. and Kaplan, D. L., *Electrospun silk-BMP-2 scaffolds for bone tissue engineering.* Biomaterials, 2006. **27**(16): p. 3115-24.

6. Williamson, M.R., Black, R., and Kielty, C., *PCL-PU composite vascular scaffold production for vascular tissue engineering: attachment, proliferation and bioactivity of human vascular endothelial cells.* Biomaterials, 2006. **27**(19): p. 3608-16.

7. Casper, C.L., Yamaguchi, N., Kiick, K. L. and Rabolt, J. F., *Functionalizing electrospun fibers with biologically relevant macromolecules.* Biomacromolecules, 2005. **6**(4): p. 1998-2007.

8. Xie, J., Li, X. and Xia, L., *Putting Electrospun Nanofibers to Work for Biomedical Research.* Macromolecular Rapid Communications, 2008. **29**: p. 17.

9. Roberts, A.B., Sporn, M. B., Assoian, R. K., Smith, J. M., Roche, N. S., Wakefield, L. M., Heine, U. I., Liotta, L. A., Falanga, V. and Kehrl, J. H., *Transforming growth factor type beta: rapid induction of fibrosis and angiogenesis in vivo and stimulation of collagen formation in vitro.* Proc Natl Acad Sci U S A, 1986. **83**(12): p. 4167-71.

10. Assoian, R.K., Komoriya, A., Meyers, C. A., Miller, D. M. and Sporn, M. B., *Transforming growth factor-beta in human platelets. Identification of a major storage site, purification, and characterization.* J Biol Chem, 1983. **258**(11): p. 7155-60.

11. Cao, L. and Mooney, D.J., *Spatiotemporal control over growth factor signaling for therapeutic neovascularization.* Adv Drug Deliv Rev, 2007. **59**(13): p. 1340-50.

12. Pierce, G.F., Vande Berg, J., Rudolph, R., Tarpley, J. and Mustoe, T. A., *Platelet-derived growth factor-BB and transforming growth factor beta 1 selectively modulate glycosaminoglycans, collagen, and myofibroblasts in excisional wounds.* Am J Pathol, 1991. **138**(3): p. 629-46.

13. Formhals, A., *Process and apparatus for preparing artificial threads, US Patent 1,975,504.* 1934.

14. Drozin, V., *The electrical dispersion of liquids as aerosols,* Journal of Colloid Science 1955. **10**(2): p. 158-164.

15. Vonnegut, B., *Production of monodisperse liquid particles by electrical atomization* Journal of Colloid Science, 1952. **7**(6): p. 616-622.

16. Simons, H.L., *US Patent 3,280,229.* 1966.

17. Taylor, G., *Electrically driven jets.* Proc. Roy. Soc., 1969. **A313**: p. 453-75.

18. Baumgarten, P., *Electrostatic spinning of acrylic microfibers.* Journal of Colloid Interface Science, 1971. **36**: p. 71.

19. Hayati, I., *Investigations into the mechanisms of electrohydrodynamic spraying of liquids. I. Effect of electric field and the environment on pendant drops and factors affecting the formation of stable jets and atomization.* Journal of Colloid And Interface Science, 1987. **117**(1): p. 205-221

20. Doshi, J., *Electrospinning process and applications of electrospun fibers.* Journal of Electrostatics, 1995. **35**: p. 151-160.

21. Fang, X., *DNA fibers by electrospinning.* J of Macromolecular Sci-Phys, 1997. **B36**: p. 169-73.

22. Li, D., *Electrospinning of nanofibers: Reinventing the wheel?* Advanced Materials, 2004. **16**: p. 1151.

23. Reneker, D.H., *Nanometer diameter fibres of polymer, produced by electrospinning.* Nanotechnology 1996. **7**: p. 216.

24. Shin, Y., *Experimental characterization of electrospinning: the electrically forced jet and instabilities.* Polymer, 2001. **42**: p. 9955.

25. Deitzel, J., *The effect of processing variables on the morphology of electrospun nanofibers and textiles.* Polymer, 2001. **42**: p. 261.

26. Zong, X., *Structure and process relationship of electrospun bioabsorbable nanofiber membranes.* Polymer, 2002. **43**: p. 4403.

27. Zhand, C.X., *Study on morphology of electrospun poly(vinyl alcohol) mats.* Eur. Polym. J, 2005. **41**: p. 423.

28. Sun, Z., Zussman, E. and Yarin, A., *Compound Core-Shell Polymer Nanofibers by Co-Electrospinning.* Adv. Mater., 2003. **15**(22): p. 1929-1932.

29. Huang, L., Nagapudi, K., Apkarian, R. P. and Chaikof, E. L., *Engineered collagen-PEO nanofibers and fabrics.* J Biomater Sci Polym Ed, 2001. **12**(9): p. 979-93.

30. Jiang, H., Fang, D., Hsiao, B. S., Chu, B. and Chen, W., *Optimization and characterization of dextran membranes prepared by electrospinning.* Biomacromolecules, 2004. **5**(2): p. 326-33.

31. Wen, Y., *Continuous carbon nanofibers for nanofiber composites.* Materials Research Society Symposium - Proceedings, 2002. **702**: p. 173-178.

32. Geng, X., Kwon, O.H. and Jang, J., *Electrospinning of chitosan dissolved in concentrated acetic acid solution.* Biomaterials, 2005. **26**(27): p. 5427-32.

33. Park, Y.H., *Characterization of gelatin nanofiber prepared from gelatin-formic acid solution* Polymer, 2005. **46**(14).

34. Beck Tan, N.C., *Controlled deposition of electrospun poly(ethylene oxide) fibers* Polymer, 2001. **42**(19).

35. Yang, Y., Jia, Z., Li, Q. and Guan, Z., *Experimental investigation of the governing parameters in the electrospinning of polyethylene oxide solution.* IEEE Transactions on Dielectrics and Electrical Insulation, 2006. **13**(3): p. 580-584.

36. Li, D. and Xia, Y., *Direct Fabrication of Composite and Ceramic Hollow Nanofibers by Electrospinning.* Nano Letters, 2004. **4**(5): p. 933-938.

37. Xia, Y., *Electrospinning of polymeric and ceramic nanofibers as uniaxially aligned arrays.* Nano Letters, 2003. **3**(8).

38. Yang, F., R. Murugan, S. Ramakrishna, et al., *Fabrication of nano-structured porous PLLA scaffold intended for nerve tissue engineering.* Biomaterials, 2004. **25**(10): p. 1891-900.

39. Hartgerink, J.D., Beniash, E. and Stupp, S.T., *Self-assembly and mineralization of peptide-amphiphile nanofibers.* Science, 2001. **294**(5547): p. 1684-8.

40. Huang, J. and Kaner, R.B., *A general chemical route to polyaniline nanofibers.* J Am Chem Soc, 2004. **126**(3): p. 851-5.

41. Ellison, C.J., *Melt blown nanofibers: Fiber diameter distributions and onset of fiber breakup.* Polymer, 2007. **48**(11): p. 3306.

42. Jiang, H., Zhao, P. and Zhu, K., *Fabrication and characterization of zein-based nanofibrous scaffolds by an electrospinning method.* Macromol Biosci, 2007. **7**(4): p. 517-25.

43. Huang, Z.M., He, C. L., Yang, A., Zhang, Y., Han, X. J., Yin, J. and Wu, Q., *Encapsulating drugs in biodegradable ultrafine fibers through co-axial electrospinning.* J Biomed Mater Res A, 2006. **77**(1): p. 169-79.

44. Jiang, H., Hu, Y., Li, Y., Zhao, P., Zhu, K. and Chen, W., *A facile technique to prepare biodegradable coaxial electrospun nanofibers for controlled release of bioactive agents.* J Control Release, 2005. **108**(2-3): p. 237-43.

45. Liao, I.C., Chew, S.Y. and Leong, K.W., *Aligned core-shell nanofibers delivering bioactive proteins.* Nanomed, 2006. **1**(4): p. 465-71.

46. Zhang, Y.Z., Venugopal, J., Huang, Z. M., Lim, C. T. and Ramakrishna, S., *Characterization of the surface biocompatibility of the electrospun PCL-collagen nanofibers using fibroblasts.* Biomacromolecules, 2005. **6**(5): p. 2583-9.

47. Zeng, J., Xu, X., Chen, X., Liang, Q., Bian, X., Yang, L. and Jing, X., *Biodegradable electrospun fibers for drug delivery.* J Control Release, 2003. **92**(3): p. 227-31.

48. Ashammakhi, N., Ndreu, A., Piras, A. M., Nikkola, L., Sindelar, T., Ylikauppila, H., Harlin, A., Gomes, M. E., Neves, N. M., Chiellini, E., Chiellini, F., Hasirci, V., Redl, H. and Reis, R. L., *Biodegradable nanomats produced by electrospinning: expanding multifunctionality and potential for tissue engineering.* J Nanosci Nanotechnol, 2007. **7**(3): p. 862-82.

49. Zhang, Y.Z., Wang, X., Feng, Y., Li, J., Lim, C. T. and Ramakrishna, S., *Coaxial electrospinning of (fluorescein isothiocyanate-conjugated bovine serum albumin)-encapsulated poly(epsilon-caprolactone) nanofibers for sustained release.* Biomacromolecules, 2006. **7**(4): p. 1049-57.

50. Ritger, P.L. and Peppas, N.A., *A simple equation for description of solute release I. Fickian and non-Fickian release from non-swellable devices in the form of slabs, spheres, cylinders or discs.* J of Controlled Release, 1987. **5**(1) p. 23-36.

51. Jia, H., Zhu, G., Vugrinovich, B., Kataphinan, W., Reneker, D. H. and Wang, P., *Enzyme-carrying polymeric nanofibers prepared via electrospinning for use as unique biocatalysts.* Biotechnol Prog, 2002. **18**(5): p. 1027-32.

52. Zhang, Y., Lim, C. T., Ramakrishna, S. and Huang, Z. M., *Recent development of polymer nanofibers for biomedical and biotechnological applications.* J Mater Sci Mater Med, 2005. **16**(10): p. 933-46.

53. Chew, S.Y., Wen, J., Yim, E. K. and Leong, K. W., *Sustained release of proteins from electrospun biodegradable fibers.* Biomacromolecules, 2005. **6**(4): p. 2017-24.

54. Li, D., McCann, J.T. and Xia, Y., *Use of electrospinning to directly fabricate hollow nanofibers with functionalized inner and outer surfaces.* Small, 2005. **1**(1): p. 83-6.

55. Kenawy, R., Bowlin, G. L., Mansfield, K., Layman, J., Simpson, D. G., Sanders, E. H. and Wnek, G. E., *Release of tetracycline hydrochloride from electrospun poly(ethylene-co-vinylacetate), poly(lactic acid), and a blend.* J Control Release, 2002. **81**(1-2): p. 57-64.

56. Ignatious, F., *Electrospun pharmaceutical compositions*, 2002: US Patent: 2003/0017208 A1.

57. Kim, K., Luu, Y. K., Chang, C., Fang, D., Hsiao, B. S., Chu, B. and Hadjiargyrou, M., *Incorporation and controlled release of a hydrophilic antibiotic using poly(lactide-co-glycolide)-based electrospun nanofibrous scaffolds.* J Control Release, 2004. **98**(1): p. 47-56.

58. Zeng, J., Aigner, A., Czubayko, F., Kissel, T., Wendorff, J. H. and Greiner, A., *Poly(vinyl alcohol) nanofibers by electrospinning as a protein delivery system and the retardation of enzyme release by additional polymer coatings.* Biomacromolecules, 2005. **6**(3): p. 1484-8.

59. Zong, X., Li, S., Chen, E., Garlick, B., Kim, K.-S., Fang, D. and Chiu, J., *Prevention of postsurgery-induced abdominal adhesions by electrospun bioabsorbable nanofibrous poly(lactide-co-glycolide)-based membranes.* Annals of Surgery, 2004. **240** (5), p. 910-915

60. Luu, Y.K., Kim, K., Hsiao, B. S., Chu, B. and Hadjiargyrou, M., *Development of a nanostructured DNA delivery scaffold via electrospinning of PLGA and PLA-PEG block copolymers.* J Control Release, 2003. **89**(2): p. 341-53.

61. Jiang, H., Hu, Y., Zhao, P., Li, Y. and Zhu, K., *Modulation of protein release from biodegradable core-shell structured fibers prepared by coaxial electrospinning.* J Biomed Mater Res B Appl Biomater, 2006. **79**(1): p. 50-7.

62. Baker, R., *Controlled Release of Biologically Active Agents.* 1987, New York: John Wiley & Sons. 279.

63. Rosenberg, R., Devenney, W., Siegel, S. and Dan, N., *Anomalous release of hydrophilic drugs from poly(epsilon-caprolactone) matrices.* Mol Pharm, 2007. **4**(6): p. 943-8.

64. Ritger, P.L. and Peppas, N.A., *A simple equation for description of solute release II. Fickian and anomalous release from swellable devices.* J of Controlled Release, 1987. **5** (1) p. 37-42.

65. Yang, Y., Li, X., Cui, W., Zhou, S., Tan, R. and Wang, C., *Structural stability and release profiles of proteins from core-shell poly (DL-lactide) ultrafine fibers*

prepared by emulsion electrospinning. J Biomed. Mater. Res. A, 2008. **86**(2): p. 374-85.

66. Yoon, J.S., *Diffusion coefficient and equilibrium solubility of water molecules in biodegradable polymers* J of Applied Polymer Science, 2000. **77**(8): p. 1716-1722.

67. Srikar, R., Yarin, A. L., Megaridis, C. M., Bazilevsky, A. V. and Kelley, E., *Desorption-limited mechanism of release from polymer nanofibers.* Langmuir, 2008. **24**(3): p. 965-74.

68. Li, T., Kildsig, D.O., Park, K., *Computer simulation of molecular diffusion in amorphous polymers* Journal of Controlled Release 1997. **48**(1): p. 57-66.

69. Saltzman, W.M. and Langer, R., *Transport rates of proteins in porous materials with known microgeometry.* Biophys J, 1989. **55**(1): p. 163-71.

70. Zeng, J., Chen, X., Liang, Q., Xu, X. and Jing, X., *Enzymatic degradation of poly(L-lactide) and poly(epsilon-caprolactone) electrospun fibers.* Macromol Biosci, 2004. **4**(12): p. 1118-25.

71. Kweon, H., Yoo, M. K., Park, I. K., Kim, T. H., Lee, H. C., Lee, H. S., Oh, J. S., Akaike, T. and Cho, C. S., *A novel degradable polycaprolactone networks for tissue engineering.* Biomaterials, 2003. **24**(5): p. 801-8.

72. Li, W.-J., Tuli, R., Okafor, C., Derfoul, A., Danielson, K.G., Hall, D.J. and Tuan, R.S., *A three-dimensional nanofibrous scaffold for cartilage tissue engineering using human mesenchymal stem cells.* Biomaterials, 2005. **26** (6), pp. 599-609

73. Wong, S.-C., Baji, A., Leng, S., *Effect of fiber diameter on tensile properties of electrospun poly(ε-caprolactone)* Polymer, 2008. **49**(21): p. 4713-4722.

74. Zhang, Y., Ouyang, H., Lim, C. T., Ramakrishna, S. and Huang, Z. M., *Electrospinning of gelatin fibers and gelatin/PCL composite fibrous scaffolds.* J Biomed Mater Res B Appl Biomater, 2005. **72**(1): p. 156-65.

75. Kim, Y.-J., Kwon, O.H., *Crosslinked gelatin nanofibers and their potential for tissue engineering* Key Engineering Materials, 2007. **342-343**: p. 169-172.

76. Choi, J.S., Leong, K.W. and Yoo, H.S., *In vivo wound healing of diabetic ulcers using electrospun nanofibers immobilized with human epidermal growth factor (EGF).* Biomaterials, 2008. **29**(5): p. 587-96.

77. Choi, J. and Yoo, H., *Electrospun Nanofibers Surface-modified with Fluorescent Proteins.* Bioactive and Compatible Polymers, 2007. **22**: p. 508-524.

78. Saraf, A., Lozier, G., Haesslein, A., Kasper, F. K., Raphael, R. M., Baggett, L. S. and Mikos, A. G., *Fabrication of Nonwoven Coaxial Fiber Meshes by Electrospinning.* Tissue Eng Part C Methods, 2009.

79. Merrill, E.W., Dennison, K.A. and Sung, C., *Partitioning and diffusion of solutes in hydrogels of poly(ethylene oxide).* Biomaterials, 1993. **14**(15): p. 1117-26.

80. Jones, S.M. and Kazlauskas, A., *Growth factor-dependent signaling and cell cycle progression.* FEBS Lett, 2001. **490**(3): p. 110-6.

81. Derynck, R., Jarrett, J. A., Chen, E. Y., Eaton, D. H., Bell, J. R., Assoian, R. K., Roberts, A. B., Sporn, M. B. and Goeddel, D. V., *Human transforming growth factor-beta complementary DNA sequence and expression in normal and transformed cells.* Nature, 1985. **316**(6030): p. 701-5.

82. Letterio, J.J. and Roberts, A.B., *Regulation of immune responses by TGF-beta.* Annu Rev Immunol, 1998. **16**: p. 137-61.

83. Ross, J.J., Hong, Z., Willenbring, B., Zeng, L., Isenberg, B., Lee, E. H., Reyes, M., Keirstead, S. A., Weir, E. K., Tranquillo, R. T. and Verfaillie, C. M., *Cytokine-induced differentiation of multipotent adult progenitor cells into functional smooth muscle cells.* J Clin Invest, 2006. **116**(12): p. 3139-49.

84. Johnston, D.E., Boughner, D. R., Cimini, M. and Rogers, K. A., *Radial artery as an autologous cell source for valvular tissue engineering efforts.* J Biomed Mater Res A, 2006. **78**(2): p. 383-93.

85. Bradford, M.M., *A rapid and sensitive method for the quantitation of microgram quantities of protein utilizing the principle of protein dye binding* Analytical Biochemistry, 1976. **72**(1-2).

86. Wang, M., *Production of submicron diameter silk fibers under benign processing conditions by two-fluid electrospinning.* Macromolecules, 2006. **39**: p. 1102.

87. Sharifpoor, S. and Amsden, B., *In vitro release of a water-soluble agent from low viscosity biodegradable, injectable oligomers.* Eur J Pharm Biopharm, 2007. **65**(3): p. 336-45.

APPENDIX A

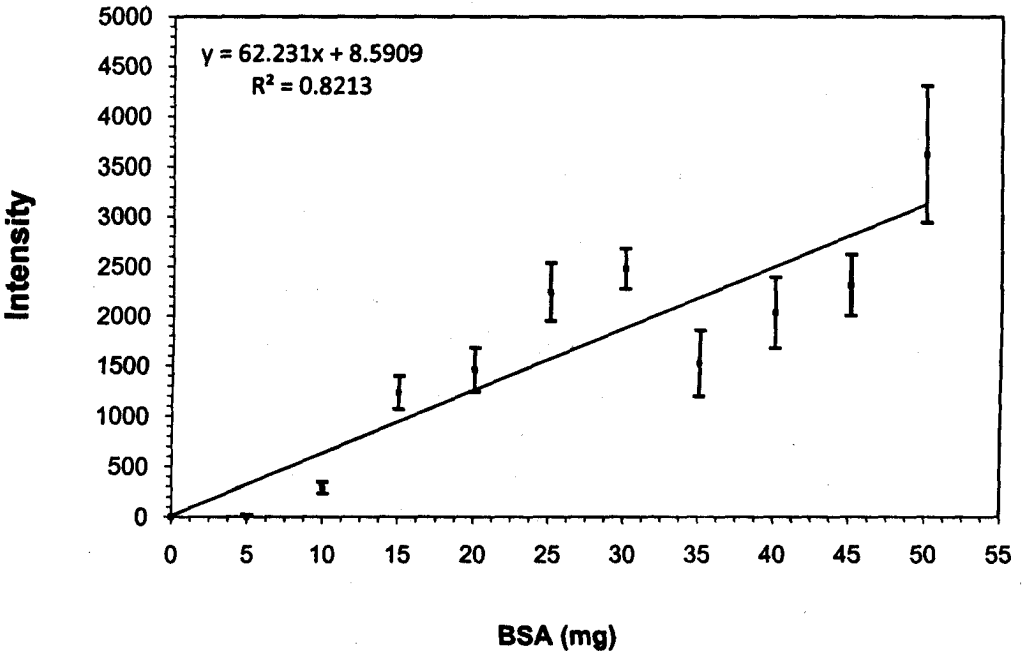

Figure 1. BSA-FITC Fluorescence Calibration Curve (Mean ± standard deviation)

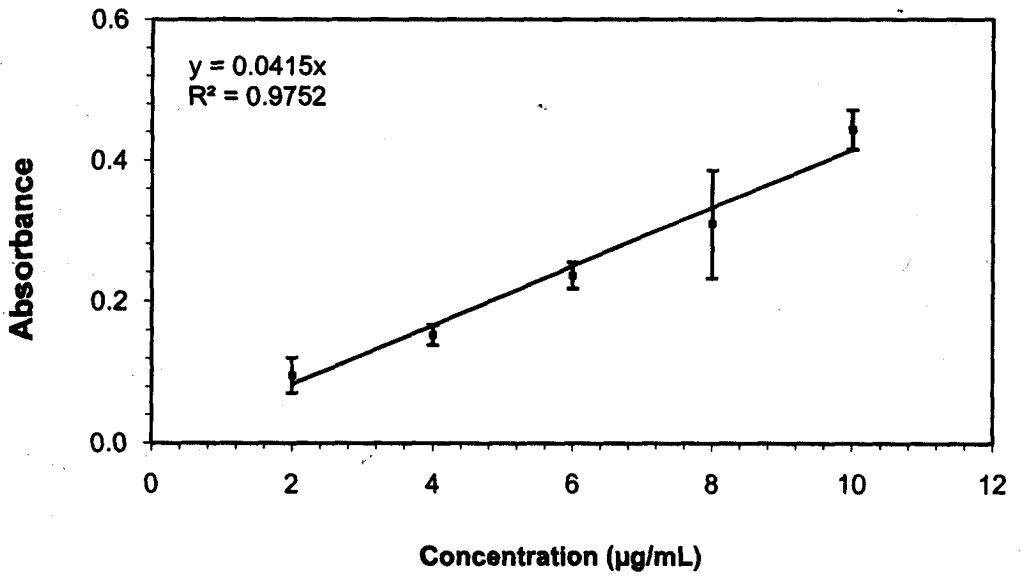

Figure 2. BSA Bradford Reagent Calibration Curve (Mean ± standard deviation)

APPENDIX B

Enzyme-Linked Immunosorbant Assay (ELISA)

In order quantify the release of growth factor from coaxially electrospun scaffolds the release of TGF-β1 can be evaluated using an extremely sensitive ELISA protein assay. In brief, a known amount of a capture antibody (MAB 240, R&D Systems) was bound to a polystyrene 96-well plate. Unbound antibody was removed by washing the plate and a blocking reagent was added. Following the wash, samples, standards and controls were incubated on the plates containing the capture antibody in order to capture the TGF-β1. The plate was then washed and a detection antibody (BAF240, R&D Systems) was added. This detection antibody was washed away and a detection reagent, streptavidin-HRP, was added. Finally, a substrate solution was added and the solutions turned blue in proportion to the amount of bound TGF-β1. Color development was stopped by the addition of H_2SO_4 and the intensity of the color in each well was measured using a micro-plate reader.

Based on the ELISA optimization experiment, the best signal to noise ratio was obtained using a capture antibody concentration of 4μg/mL and a detection antibody concentration of 400ng/mL. Using these parameters, a standard curve can be created using a series of known TGF-β1 concentrations, outlined below. Finally, this can be used to compare intensities of unknown TGF-β1 concentrations in experimental samples with known values in order to quantify TGF-β1 release from the scaffolds.

Dilution Plate

			Std 1	Std 2	2 ng/ml	5 ng/ml	10 ng/ml	50 ng/ml
Dilutions in TGF-B1 assay med			1	2	3	4	5	6
x uL sample/x uL total	A	uL TGF	30	30	200/400	200/400	200/400	200/400
dilution		uL HCl	170	170	1/2	1/2	1/2	1/2
x uL A/x uL total	B	uL TGF	25	25	200/400	200/400	200/400	200/400
dilution		uL HCl	175	175	1/4	1/4	1/4	1/4
x uL B/x uL total	C	uL TGF	20	20	200/400	200/400	200/400	200/400
dilution		uL HCl	180	180	1/8	1/8	1/8	1/8
x uL C/x uL total	D	uL TGF	15	15	200/400	200/400	200/400	200/400
dilution		uL HCl	185	185	1/16	1/16	1/16	1/16
x uL D/x uL total	E	uL TGF	10	10	200/400	200/400	200/400	200/400
dilution		uL HCl	190	190	1/32	1/32	1/32	1/32
x uL E/x uL total	F	uL TGF	5	5	200/400	200/400	200/400	200/400
dilution		uL HCl	195	195	1/64	1/64	1/64	1/64
x uL F/x uL total	G	uL TGF	2.5	2.5	200/400	200/400	200/400	200/400
dilution		uL HCl	197.5	197.5	1/128	1/128	1/128	1/128
x uL G/x uL total	H	uL TGF	0	0	200/400	200/400	200/400	200/400
dilution		uL HCl	200	200	1/256	1/256	1/256	1/256

Assay Plate

	Std 1	Std 2	2 ng/ml	2 ng/ml	5 ng/ml	5 ng/ml	10 ng/ml	10 ng/ml	50 ng/ml	50 ng/ml	BLANK	BLANK
	1	2	3	4	5	6	7	8	9	10	11	12
A	24	24	2	2	2	2	2	2	2	2	BLANK	BLANK
B	20	20	4	4	4	4	4	4	4	4	BLANK	BLANK
C	16	16	8	8	8	8	8	8	8	8	BLANK	BLANK
D	12	12	16	16	16	16	16	16	16	16	BLANK	BLANK
E	8	8	32	32	32	32	32	32	32	32	BLANK	BLANK
F	4	4	64	64	64	64	64	64	64	64	BLANK	BLANK
G	2	2	128	128	128	128	128	128	128	128	BLANK	BLANK
H	0	0	256	256	256	256	256	256	256	256	BLANK	BLANK